TECHNISCHE UNIVERSITÄT WIEN
Vienna University of Technology

Unterschrift des Betreuers

DIPLOMARBEIT

Synthesis and analysis of graphene-oxide membranes

ausgeführt an der Technischen Universität Wien
in Zusammenarbeit mit
Umeå University



Department of Physics
unter Anleitung von
Dr. Alexandr Talyzin (Umeå University, Sweden)

Betreut von
Univ.Prof. Mag.rer.nat. Dr.rer.nat. Karl Unterrainer
Institut für Photonik
der Technischen Universität Wien

durch
Thomas Hausmaninger, BSc
Josepha-Duschek-Str. 12, 5020 Salzburg

Wien, Umeå 2013

Unterschrift

List of publications and further thesis versions

This thesis is based on the following publications:

"Structure of graphene oxide membranes in liquid solvents." Talyzin, Alexandr; Hausmaninger, Thomas; You, Shujie; Szabo, Tamas, *in manuscript*

"Graphene oxide membranes in liquid water-ethanol binary solvents." Talyzin, Alexandr; Hausmaninger, Thomas; You, Shujie; Szabo, Tamas, *in manuscript*

This thesis is modified and expanded version of thesis defended at Umeå University on 17th of December.

Abstract

Graphite oxide (GO) is formed by strong oxidation of graphite. GO can be easily dispersed in single sheets of *graphene oxide*. The interest in graphene oxide was increasing in the last decade because it is one of the precursor of graphene which has many possible applications because of its outstanding electrical, mechanical and thermal properties [1]. As early as 1961 Boehm, Clauss and Hofmann studied the synthesis and properties of *graphene oxide membranes* (GO-membranes) [3]. Graphene oxide membranes consist of micrometer sized graphene oxide flakes and show selective permeability for different gases, ions and molecules. In 2012 R.R. Nair et al. reported more details about the unusual permeation properties on GO membranes [4]. Membranes with special permeation properties for different liquids and gases are used in the industries for a wide range of applications for example separation of mixtures or fuel cells.

The research goal of this work is to synthesize graphite oxide membranes out of different kinds of GO and study their properties. The kinds of GO are distinguished by the synthesis method. The membrane structure will then be studied by X-ray diffraction (XRD). Permeation properties of ethanol and water vapor reported by R.R. Nair et al. [4] should be confirmed. Furthermore permeability and filtration properties of the GO membranes for solvent water-ethanol mixtures should be investigated. The results will be compared to earlier studies done on pristine GO powder to gain more information about differences between structure and properties of GO powder and GO-membranes.

Out of three different GO materials membranes were grown using a filtration method. The structure of the membranes was characterized using XRD. Permeability for vapor of ethanol and water was tested using a gravimetric system. Furthermore filtration properties and permeability for liquid ethanol-water mixtures of the membranes were measured by vacuum filtration. With in situ XRD studies the differences between intercalation of solvents in pristine graphite oxide powder and graphene oxide membranes were investigated. Also the process of drying and reduction by heating the graphene oxide membranes was studied using XRD.

The XRD results show that the membranes consist of approximately parallel graphene oxide flakes. While permeation measurements confirm previous studies by Nair et al. on ethanol permeability they show that water permeability strongly depends on the synthesis method of the precursor GO. Measurements also demonstrate that efficiency for purification of ethanol from ethanol-water mixtures is below efficiency of other existing materials and is also depending on the kind of graphite oxide material which was used for membrane synthesis. XRD results show that water seems to be trapped in the membrane structure while in the powder structure it can move in and out more freely.

Kurzfassung

Graphit Oxid (GO) wird durch Oxidation mit starken Säuren aus Graphit hergestellt. GO kann auf einfache Art in einlagige Graphenoxid Flocken getrennt werden. Das Interesse an Graphenoxid wuchs in den letzten Jahren, da es unter anderem als ein Ausgangsstoff für Graphen dienen kann, welches wegen seiner besonderen elektrischen, mechanischen und thermischen Eigenschaften eine Vielzahl von möglichen Anwendungen hat [1]. Schon 1961 untersuchten Boehm, Clauss und Hoffmann die Synthese und Eigenschaften von Graphenoxidmembranen. Graphenoxidmembrane bestehen aus Mikrometer großen Graphenoxidflocken und zeigen selektive Durchlässigkeit für verschiedene Gase, Ionen und Moleküle. 2012 veröffentlichte R.R. Nair et al. detailliertere Ergebnisse bezüglich der ungewöhnlichen Filtereigenschaften der Graphenoxidmembrane. Membrane mit spezifischen Filtereigenschaften für verschiedene Flüssigkeiten und Gase können in der Industrie in vielen Bereichen angewandt werden.

Das Forschungsziel dieser Arbeit ist die Synthese und Analyse von Membranen aus unterschiedlichen Graphitoxidproben. Die Graphitoxidproben unterscheiden sich durch die Synthesemethode mit der sie hergestellt wurden. Die Membran Struktur wird anschließend mittels Röntgenbeugung (XRD) untersucht. Die Ergebnisse von R.R. Nair et al [4] bzgl. Durchlässigkeit der Graphenoxidmembrane für Wasser- und Ethanol Dampf sollen bestätigt werden. Außerdem sollen die Filtereigenschaften der Graphenoxidmembrane für Wasser-Ethanol Mischungen in flüssiger Form untersucht werden. Die Ergebnisse werden dann mit früheren Untersuchungen von GO-Pulver verglichen, um mehr Informationen über die Unterschiede zwischen GO-Pulver und Grapheneoxidmembranen zu gewinnen.

Graphenoxidmembrane aus drei unterschiedlichen GO-Proben wurden mittels einer Filtermethode hergestellt. Die Membranstruktur wurde mittels XRD untersucht. Die Durchlässigkeit für Ethanol und Wasserdampf wurde mittels einer gravimetrischen Methode getestet. Die Filtereigenschaften und Durchlässigkeit der Membrane für Ethanol-Wasser Mischungen wurden mittels Vakuumfiltration gemessen. Mit in-situ XRD-Untersuchungen wurden die Unterschiede zwischen Graphenoxidmembranen und GO-Pulver beim Eindringen von Flüssigkeiten sichtbar gemacht. Zusätzlich wurde der Prozess der Austrocknung und Reduktion durch Erhitzen der Membrane mittels XRD untersucht.

Die XRD Ergebnisse zeigen, dass die Graphenoxidmembrane aus in etwa parallel ausgerichteten Graphenoxid flocken bestehen. Während die Ergebnisse bezüglich Durchlässigkeit von Ethanol Dampf von Nair et al. bestätigt wurden, wurde gezeigt, dass die Wasserdurchlässigkeit stark von der Synthesemethode des für die Membranherstellung verwendeten GO abhängt. Aus den Messungen geht hervor, dass die Effizienz der Trennung von Ethanol-Wasser Mischungen weit unterhalb von industriell verwendeten Materialen liegt. Die XRD Ergebnisse zeigen mehrfach, dass Wasser in der Membranstruktur deutlich stärker gebunden ist als in GO-Pulver.

Acknowledgement

This project would not have been possible without the support of many people. First and foremost, I would like to thank my supervisor, Dr. Alexandr Talyzin, for sharing his knowledge, guidance and advice. He spent a lot time to talk over experiments and to discuss and interpreted the results. I am also very grateful to Shujie You for helping me with the XRD measurements and for sharing her lab experience with me. I also appreciate a lot the help of Lena Åström with solving technical problems in the workshop. Thanks go also to Dr. Hamid Reza Barzegar Goltapehei for helping with the membrane reduction by LASER light and to Nicolas Boulanger for spending several hours recording the UV/Vis absorption spectra with me. I also want to mention the helpfulness in daily life of all the other staff of the Umeå University Physics Department. Special thanks go to Dr. Tamás Szabó from University of Szeged for providing the Brodies GO sample. Andrey Shchukarev from the Department of Chemistry should be acknowledged for recording XPS spectra, Dr. Per Hörstedt from the Department of Plant Physiology for recording the SEM images and Dr. Diana Thomas for the help with XRD experiments performed at MAX-IV laboratory.

Thanks to Professor Karl Unterrainer for agreeing to supervise the thesis at the Technical University Vienna. My special thanks go to Professor Roger Halling as ERASMUS coordinator at Umeå University and as Professor Maria Ebel as ERASMUS coordinator at TU-Vienna for helping me to find a supervisor and their quick responses to all my questions.

My very personal thanks go also to my sisters and brothers for always reminding me to enjoy my years of study and my life. Also many thanks go to all my friends who are around in good and in bad times. Especially without the company and help of my fellow students my studies would not have been so smooth and joyful.

Dedicated to my parents, for their enduring support.

Contents

List of publications and further thesis versions 2
Abstract 3
Kurzfassung 4
Acknowledgements 5
Contents 6
1 Introduction 8
1.1 Synthesis methods graphite oxide 8
1.2 Graphene oxide structure 8
1.3 Graphite oxide solvation and hydration 10
1.4 Graphene oxide single sheets 12
1.5 Graphene oxide membranes 12
2 Experimental methods 14
2.1 Membrane fabrication procedure 14
2.1.1 Graphene oxide Solutions 14
2.1.2 Synthesis of the membranes 15
2.2 Testing Liquid permeation test of liquid ethanol/water mixtures trough the graphene oxide membranes. 17
2.3 Vapour permeation test 19
2.4 X-ray diffraction 20
2.4.1 Introduction to crystallography 20
2.4.2 Laue equation 21
2.4.3 Bragg's law 23
2.4.4 Interstratification and Méring's principles 24
2.4.5 Radiation from X-ray tubes 25
2.4.6 Synchrotron radiation for XRD 25
2.4.7 Crystal structure of graphite 26
2.4.8 X-Ray Diffraction geometries 28
2.4.9 X-Ray Diffractometer Siemens D5000 28
2.4.10 Synchrotron MAX II Beamline 711 29
3 Results and discussion 31
3.1 Synthesis 31

3.1.1 Graphene oxide Solutions 31
3.1.2 Deposition of membranes using different precursory GO Solutions 31
3.2 SEM imaging 33
3.3 XRD analysis 37
3.3.1 H-GO Membrane immersed in water 41
3.3.2 Reduced membranes 43
3.3.3 Membrane immersed in ethanol 45
3.4 Membrane characterization by other methods 48
3.5 Vapour permeation 48
3.6 Permeation of liquid ethanol water mixture in filtering experiments 52
4 Summary and conclusion 56
5 Appendix 58
5.1 Data of GO solutions 58
5.2 Data of Membranes 58
6 References 60

1 Introduction

Membranes with special permeation properties for different liquids and gases are used in the industries for a wide range of applications for example for separation of mixtures or in fuel cells. *Graphite oxide (GO)* (also earlier called for example graphic acid [5] or graphitic oxide [6]) is used for materials which are formed by strong oxidation of graphite. GO can be dispersed in singlesheets of *graphene oxide* [3],[7] ,[8]. As early as 1961 Boehm, Clauss and Hofmann studied the synthesis and properties of *graphene oxide membranes* (GO-membranes) [3]. In 2012 R.R. Nair et al. reported more details about the unusual permeation properties on GO membranes [4].

The **research goal** is to synthesize membranes out of different kinds of pristine GO and study their properties. This includes the attempt to confirm the permeation properties of ethanol and water reported by R.R. Nair et al. Furthermore the permeability of GO membranes for water-ethanol mixtures should be investigated. The membrane structure will be studied by XRD. To gain more information about the differences between the powder and membrane structure the results will be compared to earlier studies done on GO powder.

1.1 Synthesis methods graphite oxide

The graphite oxide samples used for the experiments in this thesis were prepared by two different synthesis methods:

- Brodie method [5]: For oxidation of the graphite Brodie used a mixture of potassium chlorate ($KClO_3$) and strong fuming nitric acid (HNO_3). After oxidation the GO was washed with a large amount of water and repeated the oxidation process for several times. Many variations of this method exist. For example L. Staudenmaier added the $KClO_3$ in several steps rather than at once [9]. The GO powder sample used in our studies was provided by Tamás Szabó, see details of synthesis elsewhere [10]. It follows the original procedure except for use of $NaClO_3$ instead of $KClO_3$. This sample will be referred to as *Brodies GO (B-GO)* in this thesis.

- Hummers and Offeman method: Oxidation was performed using [6] a water-free mixture of sulphuric acid (H_2SO_4), sodium nitrate ($NaNO_3$) and potassium permanganate ($KMnO_4$). Water and hydrogen peroxide were used to wash the GO after the oxidation process. The material synthesised by this method is referred to as *Hummers GO (H-GO)* within this thesis.

1.2 Graphene oxide structure

The hexagonal layered structure of graphite (see section 2.4.7) can also be observed in GO, although due to the oxidation the structure becomes strongly disordered [10]: The interlayer spacing increases from 3.4 Å of pristine graphite to ~6 Å and the layers get rippled. Although the name “graphite oxide” does not reflect complex composition of this material, a variety of functional groups are attached to graphene sheets, both on the edges and on the planes. The detailed structure of the GO and especially the graphene oxid sheets is still discussed and various measurement results show that the structure is strongly depending on the method of synthesis [10].

Early models proposed by Hofmann, Ruess, Sholz-Boehm and Nakajima Matsuo were based on a regular lattice structure [2].

Lerf and Klinowski more recently proposed that GO is a nonstoichiometric compound (see Fig. 1) [11]: Lerf and Klinowski built their model based on measurements with nuclear magnetic resonance (NMR) spectroscopy. A sample prepared by Hummers method was studied and C-OH groups, C-O-C and >C=C< groups in the bulk of GO were detected. With infrared spectroscopy also a low quantity of carboxylic acid groups was detected which might be on the periphery of the graphitic platelets of GO [2].

A structural model suggested by Szabó is based on measurements of B-GO [10]: It is based on a corrugated carbon network and also includes C=O species on the basal plane (see Fig. 1 (C)).

The structural difference between the B-GO and H-GO sample used in this thesis were confirmed by recent XRD, FT-IR, Raman spectroscopy and XPS measurements [12]: The interlayer distances measured with XRD at ambient conditions was for B-GO 6.35 Å and for H-GO 7.18 Å which also could be the result of different hydration of the samples. FT-IR spectra give information about the chemical functionalities and shows that B-GO includes a higher relative amount of C-OH groups and H-GO a higher amount of C=O groups. The XPS spectra show general a more complex functional composition of the H-GO sample compared to B-GO. Furthermore Hydration and solvation experiments observed indicate more crystallinity of the B-GO samples (see also section 1.3)[12].

Near-edge X-ray absorption fine-structure and transmission electron microscopy on few-layer-GO give more insight on the electronic structure of GO [13]: The measurements show that sp^2 hybridization of the carbon atoms like in graphene and graphite dominates and a strong decoupling between the layers is indicated. Furthermore also partly sp^3 hybridisation was detected with locally different intensity. This can be seen as locally variation of oxidation-degree on a scale of a few nm, which was also confirmed by Photoelectron emission microscopy measurements.

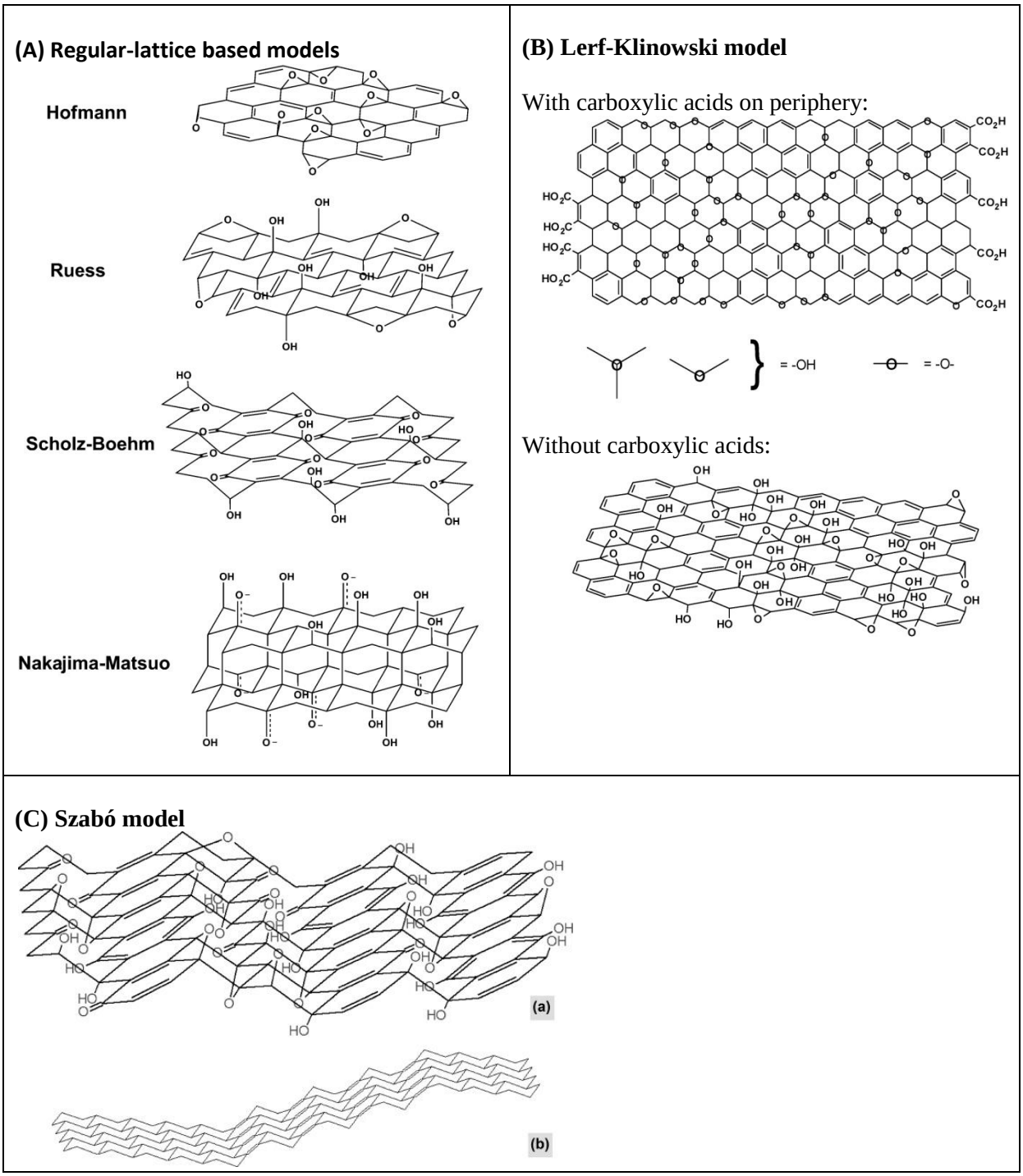


Fig. 1 Old lattice based models (A) versus the newer non-stoichiometric Lerf-Klinowski mode (B), ref. [2] and the Szabó model (C) with the corrugated carbon network (b), ref. [10].

1.3 Graphite oxide solvation and hydration

Unlike pristine graphite, the GO is hydrophilic and gets intercalated by water and other polar solvents when exposed to vapour or liquid. After being exposed to liquid water the interlayer distance of GO increases to approx. 12 Å [14][15]. Similar behaviour can be observed for example with mineral clays [16]. The following gives some examples on effects which were observed for GO immersed in different polar solvents.

Studies with broadband dielectric spectroscopy (BDS) and Fourier transform infrared spectroscopy (ATR-FTIR) show, that the water dynamics and behaviour change with concentration of water in the B-GO [17]: For concentration lower 17 wt% the water molecules have low rotational freedom and seem to be strongly bound to the graphene layers. For concentrations higher than 17 wt% the rotational freedom increases. For concentration higher than 30 wt% water crystallisation could be measured with differential scanning calorimetry around the freezing point of water. Below about 30 wt% the water seems to stay amorphous also below the freezing point.

Lerf et Al. also studied H-GO samples using NMR spectroscopy (CP-MAS) [18]: For fully hydrated H-GO samples two lines in the ^{1}H-NMR spectrum were found where one can be assigned to water which is strongly bound by the GO structure and the other to mobile water. In further neutron TOF studies on hydrated GO samples prepared by Brodies and Staudenmaiers method three types of motion were identified [15]: Two kinds of slow motion where one was assigned to rotational or flipping motion of isolated water molecules and the other could not be clearly identified. Again only samples exposed to air with 100% relative humidity showed additional translational motion of water molecules.

Further studies using quasielastic neutron scattering show this two kinds of slow water motion in hydrated B-GO [14]. The motion of strongly bound water molecules is explained by a two-site jump model as shown in Fig. 2 which combines flipping motion of bound water molecules and OH groups.

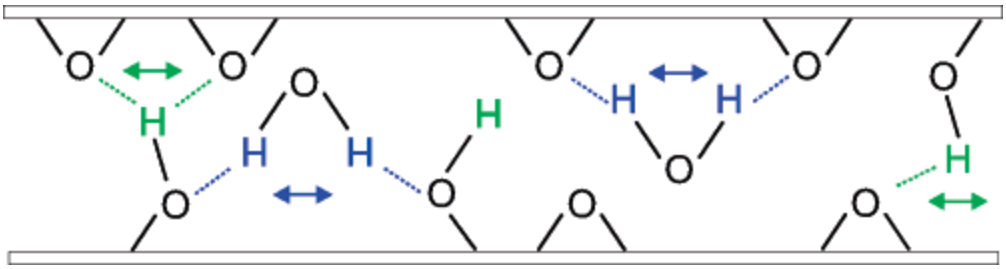


Fig. 2 Model of strongly bound water molecules and OH-groups. The two layers of the carbon grid on the top and bottom of the figure are presented flat for simplification. (Figure reference [14])

Furthermore XRD studies show a strong dependence of the degree of hydration on the kind and aging of the GO [15],[14]. The time for expanding interlayer distance to its maximum amount (10.5 Å) after being exposed to saturated humid air was between 4 days to 4 weeks. Some samples even had to be immersed in water to reach the maximum expansion.

XRD study of water saturated B-GO and H-GO samples at ambient temperature showed that the interlayer distance increases by 4.1 Å for B-GO and by 5.2 Å for H-GO [12]. This increase of inter-layer distance corresponds to thickness between one monolayer and two monolayers of water. The measured position of XRD peak could be the result of inhomogeneous intercalation of various GO flakes which show partly intercalation of one monolayer and partly two monolayers of water between the GO layers. The random combination of layers hydrated with different number of water monolayers (interstratification) results in appearance of single peak on XRD with position determined by relative number of single and two layer hydrates (see section 2.4.4).

B-GO immersed in excess of other polar solvents, e.g. methanol, reveals a different behavior [19][20]: methanol and ethanol are intercalated in exactly one monolayer under ambient conditions. Sharp phase transition can be observed upon cooling the system and a second monolayer is inserted. The phase transition is complete for B-GO in methanol, but for ethanol this phase-transition occurs only for part of sample as revealed by XRD. The results of DSC measurements on B-GO samples saturated with water-methanol mixtures showed that mixtures with over 45% water will most likely not lead to this sharp phase transition [21]. A sharp phase transition due to insertion of a second monolayer of ethanol or methanol can also be observed at a pressure of 0.3-0.8 GPa. Though for H-GO similar sharp phase transitions could not be observed [12].

1.4 Graphene oxide single sheets

The solubility in water is also different for H-GO and B-GO. H-GO can be dissolved in pure water using soft sonication for several hours and the dispersabilitiy of H-GO is in the order of 1-4 mg/ml [22]. For B-GO even prolonged sonication dose not result in formation of stable dispersions. However, B-GO can be dispersed in water even without sonication in slightly basic solutions (approx. 0.01 mol/l NaOH) [3].

Evidence of single sheets in solutions of H-GO powder which was dispersed by sonication was given using AFM [8],[23],[24],[25] as well as for B-GO [7]. The graphene oxide flakes sizes are in the order of several µm [26].

The thickness of the single graphene oxide flakes is approx. 1-1.4 nm which is thicker compared to graphene (~0.34 nm) due to the functional groups attached [27],[28] (see also section 1.2).

1.5 Graphene oxide membranes

As early as 1961 Boehm, Clauss and Hofmann studied "graphite oxide and its membrane properties" [3]: B-GO was dissolved using 0.01 mol/l sodium hydroxide solution and then slowly evaporated the water on a glass plate, where "paperlike foils" were obtained. The measurements showed that they have "good mechanical strength" and are "not permeable for gases like nitrogen or oxygen", but permeable for water. A permeation of 0.1 mg/min·cm² with a partial water-vapour pressure of 23 mm Hg (≈3 kPa) was measured.

In 2007 Dikin et al. reported synthesis of H-GO "paper" by filtering a dispersion of GO flakes, which resulted in samples with a thickness of 1 to 30 µm [27]. The paper showed an interlayer-spacing of about 8 Å. The stress-strain curves reported in this study showed behavior similar to paper, including a straightening, linear (elastic) and plastic regime. There was no pull-out of the GO lamellae observed which can be seen as the result of good material homogeneity and a strong binding between the layers. They suggest that the rippled GO structure leads to a good load distribution across the whole sample.

Self-assembled graphene oxide membranes were also made on a liquid/air surface by heating the GO solution [29]. An H-GO water solution (with a concentration of about 1-3 mg/ml) was heated to 353 K so that a thin GO film condensed on the liquid/air surface. Within 10-40 min membranes of the thickness 5-10 µm grew. The membranes were more uniform if they were

grown faster (with higher heating temperatures and concentrations). Also it was detected that membranes were not transparent for UV-light, but for the visible region the transparency increased strongly with decreasing thickness. Furthermore these membranes showed mechanical properties similar to those measured by Dikin et al. for filter grown membranes [27].

A similar method with evaporating water from a GO solution-droplet and growing thin membranes for so called “E-cells” for electron microscopy was also suggested recently [30]. GO is convenient for this purpose because the windows of these E-cells should be transparent for electron beams but gas leak-tight.

Since graphene shows extraordinary electronic properties [1] also the electronic properties of graphene oxide and reduced graphene oxide membranes is of interest. Therefore ultrathin membranes of one or more monolayer of graphene oxide and reduced graphene oxide were grown by different techniques: Zuh et al. made monolayers chemically reduced graphene oxide in the solution and fabricated centimeter-area conducting films by dipcoating [8]. Kovtyukhova et al. synthesized monolayer GO films on ITO wavers which were covered with a cationic monolayer to attract the GO, the coated wavers were immersed in a GO solution and then rinsed with water [24]. Also other techniques like drop-casting [25], spraying on a preheated substrate [31] or spin coating[23][32] , spin coating in combination with nitrogen drying and suspending in methanol [33] as well as electrophoresis of reduced GO solutions[34] were used to produce thin films for electrical conductivity testing. The results show that the GO films can be made insulating, semiconducting as well as semimetallic depending on the method of deposition and grade of reduction [35].

More recent papers also show properties of GO membranes like selective ion permeation [36] or possible application in fuel cells [37]. Also the ability to filter some organic molecules has been shown [38].

In 2012 R.R. Nair et al. reported unusual permeation properties on H-GO membranes [4]. It was shown that the permeability of the membranes for helium is below 10^{-15} g·mm/cm²·s·bar. Also for several other gases like for argon, hydrogen, nitrogen measurements showed an upper limit for the permeation rate at 10^{-12} g·mm/cm²·s·bar. Furthermore experiments with vapor of ethanol, acetone, hexane gave the result that the permeation-rate is below 10^{-11} g·mm/cm²·s·bar for these vapors. In sharp contrast, the water vapor permeates through the membrane nearly as fast as through an open hole. Nair et al. explains this permeation with a model of capillaries of not oxidized areas (see Fig. 3).

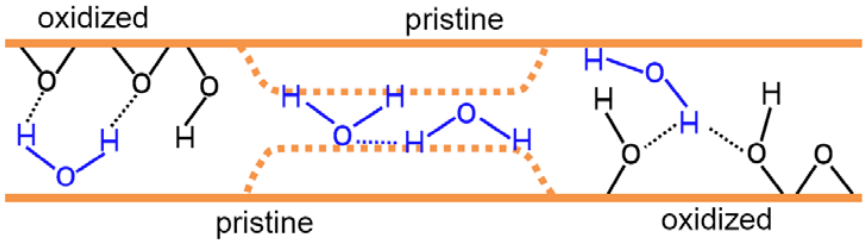


Fig. 3 Model of graphene capillaries by Nair et al. (figure reference [4]).

2 Experimental methods

2.1 Membrane fabrication procedure

2.1.1 Graphene oxide Solutions

The Hummers-GO samples of "ACS Material Single Layer Graphite oxide" (SL-H-GO) and "ACS Material Graphite oxide" (H-GO) were purchase at the manufacturer ACS Material, LLC. The Brodies-GO (B-GO) was kindly providet by Tamás Szabó. For previous studies of these samples see ref. [12], [21], [19], [20].

Hummers-GO is soluble in pure water with the help of sonication. To 1 ml H_2O about 1 ml H-GO was added and then sonicated in an ultrasonic bath for about 24 hours. After this the solution was centrifuged for 1 hour with 8000 RPM. Then the solution was separated from the not dissolved GO.

Brodies-GO is not soluble in pure water. Therefore we used a NaOH in water solution with a concentration lower than 0.1 mol/l instead of pure water as proposed by Boehm et Al.[3]. The solution is not so stable. With prolonged centrifugation and also after some days of storing it gets more precipitate. For growing the membranes the solution was centrifuged with 4400 RPM for 30 minutes.

The concentration of the solutions was measured as followed: A small amount of solution was put in a glass vial and then the water was slowly evaporated in low vacuum. The weight of the glass vial (m_v), vial+solution (m_{vs}) and of the vial+dry GO (m_{vg}) was measured carefully with a laboratory balance and then the concentration in mass per volume (c) was calculated as follows

$$c = \frac{(m_{vg} - m_v)}{(m_{vs} - m_{vg})\rho_w} = \frac{m_{GO}}{\rho_w \cdot m_{solution}}$$

Where ρ_w is the density of water at room temperature ($\rho_w = 1$ g/ml).

To see the effect of contamination with dust or condensed water also a test-vial was measured: The test-vial filled with distilled water was put in the vacuum chamber together with the vial containing the solution. The vial was weighted in empty state before and after the evaporation of the water. The weight of the test-vial did not change more than 0.1 mg. Also the weight of vials with the precipitate did not change more than 0.1 mg after prolonged storing. The precision of the balance was also 0.1 mg. Therefore the error of the weight-measurements can be assumed to be Δm=0.1 mg.

The resulting Error of the concentration with the approximation that $|m_{vg} - m_v| \ll |m_{vs} - m_{vg}|$ and $|m_{vs} - m_v| \approx |m_{vs} - m_{vg}|$ is:

$$\Delta c = \frac{|\Delta m|}{\rho_w}\left(\frac{|m_{vs}-m_v|+|m_{vs}-m_{vg}|+|m_{vg}-m_v|}{(m_{vs}-m_{vg})^2}\right) \approx \frac{|\Delta m|}{\rho_w}\left(\frac{2}{|m_{vs}-m_{vg}|}\right) \approx \frac{|\Delta m|}{\rho_w}\left(\frac{2}{|m_{solution}|}\right)$$

For concentrations between 0.5 and 11 mg/ml the resulting error is: Δc=0.2 mg/ml for 1 ml of solution, Δc=0.1 mg/ml for 2 ml and Δc=0.06 mg/ml for 3 ml of solution.

It should be noted that the water intercalated in the precipitate is also a part of the resulting concentration.

2.1.2 Synthesis of the membranes

The membranes were grown by filtering the GO solution trough Anodisc membranes (Anodisc 25, 0.2 µm, diameter: 25 mm from Whatman GmbH) as shown in **Fig. 6.1**. The filter holder (see **Fig. 5**) was connected to a vacuum flask using a rubber bung. In the vacuum flask an under pressure was established by pumping the air with a vacuum pump. The rate of GO deposition on the filter depends on the rate of solution filtration which was controlled by using a valve between pump and vacuum flask (see **Fig. 4**).

The grid in the top part of the anodisc-filterholder can be removed (see **Fig. 5 (B)**). This has the following advantages: it is possible to observe the filter paper in process of the membrane growing and secondly when removing the top-part of the filter the grid can cause harm to the membrane because of the small distance between the grid and the membrane and the remaining solution. Furthermore the top-grid can cause an impress in the membrane if it is too thick (see **Fig. 7 (B)**). In case the whole solution needs to be filtered and no solution must be left on the membrane it is better to use the grid. This is because the grid prevents the solution from forming droplets at the border of the membrane and filter holder which might cause inhomogeneities particularly for B-GO membranes.

The speed of membrane growing is affected by the under-pressure created by pumping (especially in the first minutes when starting growing the membrane and also more for H-GO membranes then for B-GO membranes) and needs to be carefully controlled using the valve. When the syringe with the GO solution was empty it was filled with 2ml water so that the rest of the GO solution left in the filter holder also could be filtered without forming a droplet on the membrane and making it inhomogeneous (see **Fig. 7 (C)**).

Diluting the H-GO solution with 1 part of saturated solution + 1 part H2O and further 15 min sonication bath lead to more homogenous membranes. Without diluting the membranes grew within about 2 hours and most of the times had a more transparent (thinner) spot or even a hole in the central part (see **Fig. 7 (A)**).

For drying the membranes were put (together with the Anodisc filter) on a dust-free paper and covered with a plastic cap for dust protection. For B-GO membranes it easily happened that there appeared some inhomogenities during the drying process if the water was withdrawn by the paper below the filter only on small areas (see **Fig. 7 (D)**).



Fig. 4 Valve used for controlling the flow rate of the vacuum pumping.

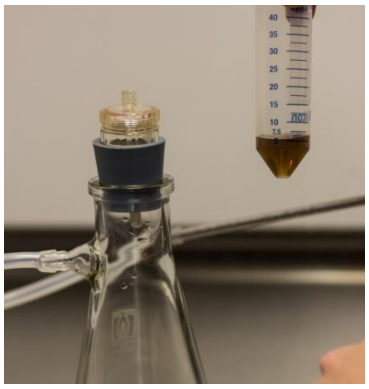
(A) (B)



Fig. 5 Opened filterholder (A) and the toppart of filterholder with disasambled grid (B).



1. Put membrane on filter holder



2. Add (diluted) GO Solution to filter holder and syringe



3. Start pumping and filtering the GO solution

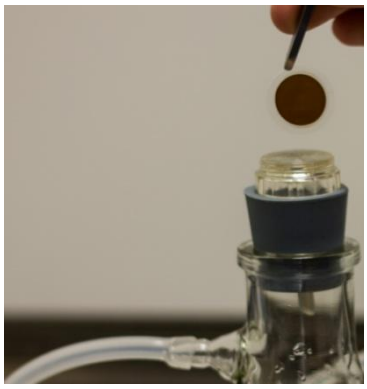


4. Add 2ml water when syringe is empty.





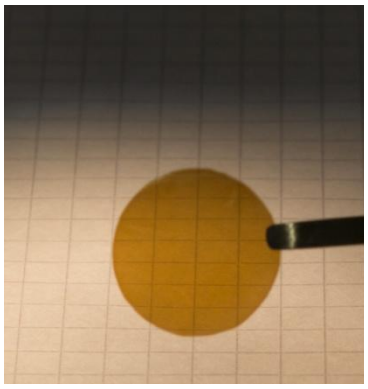
5. After syringe is emptied again remove filter holder and rest of water



6. Remove filter with membrane.



7. Let membrane dry



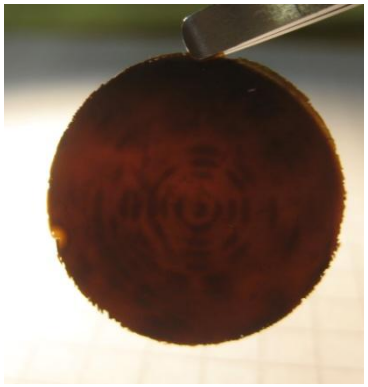
8. Remove membrane from filter

Fig. 6 Synthesis of GO membranes

(A) SL-H-GO



(B) H-GO



(C) H-GO



(D) B-GO



Fig. 7 Different kinds of inhomogeneities: (A) SL-H-GO membrane with typical flaky structure and a hole in the middle caused by too strong under-pressure below the filter. (B) Thick H-GO membrane with structure of top-grid of filter. (C) H-GO membrane with in homogeneity due to partly coverage with solution in the end of the growing process. (D) B-GO membrane with inhomogeneity caused in the process of drying.

2.2 Testing Liquid permeation test of liquid ethanol/water mixtures trough the graphene oxide membranes.

Simple permeation tests for water-ethanol mixtures were directly performed using the setup for growing the membranes (see **Fig. 8**). After the membrane had been grown a water-ethanol

mixture was put in the syringe. Note that the vacuum flask needs to be dried to avoid water evaporation which results in a lower vacuum. Then the valve was opened several turns to start a vacuum in the flask. Solution which passes through the membrane is then evaporating from the bottom of the anodisc filter. No liquid droplets were observed on the bottom size of the filter which is possible only if the rate of liquid permeation trough the membrane is slower compared to the rate of evaporation from the surface of filter.

When 2 ml of solution had permeated through the filter the water ethanol mixture was considered to have approximately the same concentration in the filter holder and the syringe. It is possible, because the concentration of ethanol increases with time near the filter and therefore it should mix with the liquid in the syringe because the density of ethanol is lower than that of water.

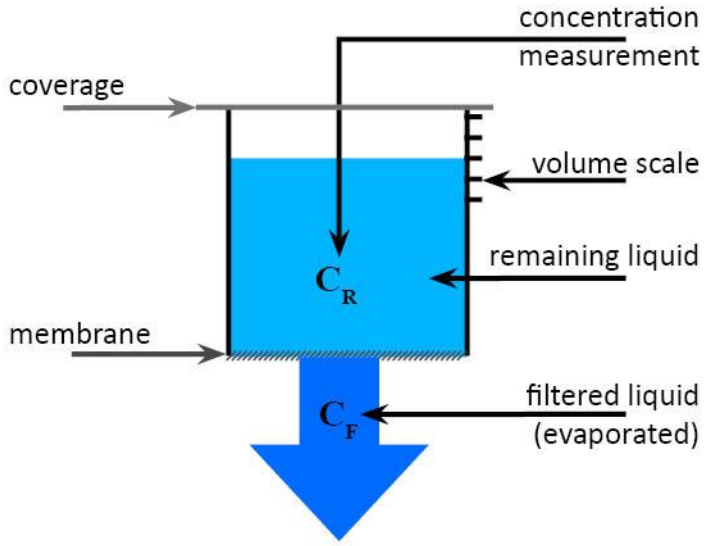


Fig. 8 Experimental setup for permeation of liquid water/ethanol mixture through GO membrane.

The *concentration* of ethanol in the mixture was measured with the density meter "Mettler Toledo Densito 30PX" which provides a precision of ±1%vol ethanol according to specifications.

The *volume* change of the whole mixture was measured using the scale on the syringe. For the measurement with the H-GO Membrane a 50ml-syringe with a 1ml-scale-division was used and the error of the volume measurement can be considered as +/-0.5 ml. For the B-GO Membrane a 5ml-syringe was used with a 0.2ml-scale division and the error can be considered as +/-0.1 ml.

Additional volume of the filter holder and the lower part of the syringe has to be considered: For the filter holder (without top-grid) a volume of 1.9 ml was measured and 2.1ml for the

50ml-syringe and 0.2ml for the 5ml-syringe. This can lead to a systematic error of max. 0.3ml which is not relevant for the qualitative measurements made.

The *time* was recorded with a precision of approx. 5min which can be neglected due to the fact that the measured time spans are mostly more than 10 hours.

One permeation-rate measurement consists of two steps (1,2) which both include a measurement of volume (V_1, V_2), ethanol concentration (C_1,C_2) and point of time (t_1,t_2). The concentration measurement changes the volume in the syringe. Therefore, for the next permeation-rate measurement the same concentration and time can be taken as for the first measurement point ($C_{2_old} \rightarrow C_1$, $t_{2_old} \rightarrow t_1$), but a different volume has to be recorded.

The following data were calculated out of these measurements:

- Volume of total mixture permeated through the membrane ($\Delta V = V_1 - V_2$)
- Volume of ethanol permeated ($\Delta V_E = C_1 V_1 - C_2 V_2$)
- Permeation rate ($r = \Delta V / \Delta t$)
- Average ethanol **concentration of remaining mixture** ($C_R = \bar{C} = (C_1 + C_2)/2$)
- Ethanol **concentration in mixture filtered** through the membrane ($C_F = \Delta V_E / \Delta V$)

The error limits for these quantities were calculated by error propagation methods out of the error estimation for volume and concentration measurement made above.

All concentrations were measured and calculated in units of volume percent of ethanol.

2.3 Vapour permeation test

For measuring the vapour permeability of water and ethanol through the membrane the weight loss of a vial half filled with the liquid and closed by the membrane was measured. The weight-loss corresponds directly to the vapour permeated through the membrane.

For the weight-change measurement over time a magnetic suspension balance of Rubotherm was used. This balance makes a zero-point correction after every measurement point which results in a reproducibility of approximately ±0.02mg [39]. Since the measurements were recorded over long time with many measurement points the noise is eliminated by averaging and does not contribute to the results presented here.

Glass-vials with metal caps and rubber discs for sealing were used. In the cap and the rubber disc a hole was stamped (see **Fig. 9**). For gluing the membranes on the top of the cap two different glues were used: silicon sealant (Dana Lim A/S Universal Silicone) and Epoxy (Loctite Power Epoxy). The advantage of silicone was that it was easy to handle and also after hardening elastic enough to protect the membranes from breaking. However it turned out, that the silicon is not sealing good enough for our measurements. The Epoxy is not elastic after hardening and if too much force came on the membrane (for example due to pressure increase in the bottle) it started to peal of the epoxy. Therefore to stabilize the membrane the epoxy was also applied on top of the membrane together with a lining disk (see **Fig. 10**). Also a combination of silicone and Epoxy was tried where the silicone was used to protect the

membrane from the sharp edges of the hole (see **Fig. 9** (A)), but it turned out that some of the silicone intercalates between the epoxy used for gluing the membrane and the metal cap.

The main error of the measurement comes from leaking of the bottle and the glue which was used to glue the membrane on the bottle. To estimate this systematic error instead of the membrane an aluminium foil was glued on top of the cap one time using silicon sealant and one time epoxy. A measurement with ethanol in the vial gave a rate of $1.1 \cdot 10^{-6}$ g/min for the foil glued with silicone and a rate lower than $1.5 \cdot 10^{-7}$ g/min for the foil glued with epoxy.



Fig. 9 Evaporation vial: (A) cap with open hole, (B) bottom view of cap, (C) vial, ready for measurement, with membrane glued on top and liquid inside.



Fig. 10 Membrane glued with epoxy together with a lining disk to keep the epoxy away from the membrane over the hole.

2.4 X-ray diffraction

X-ray radiation can be used for structural characterization of crystalline compounds. The following section gives an introduction into crystallography and the basics of X-ray diffraction (XRD).

2.4.1 Introduction to crystallography

For an ideal crystal lattice with translational symmetry three linearly independent *lattice vectors* $(\boldsymbol{a_1}, \boldsymbol{a_2}, \boldsymbol{a_3})$ exist which are defined such that the point $\boldsymbol{r}$ is equivalent to the point $\boldsymbol{r'} = \boldsymbol{r} + u_1\boldsymbol{a_1} + u_2\boldsymbol{a_2} + u_3\boldsymbol{a_3}$ where u_1, u_2, u_3 are integers [40]. The set of all possible points $\boldsymbol{r'}$ form a *lattice*. A smallest possible unit cell $V = \boldsymbol{a_1} \cdot (\boldsymbol{a_2} \times \boldsymbol{a_3})$ for a specific crystal lattice is called a *primitive cell*. A special primitive cell is the Wigner-Seiz cell: it is defined as the polyhedral which is constructed by drawing planes that bisect lines joining each atom to its nearest neighbours [40]. To completely describe an ideal crystal a *basis* of atoms is

"attached" to each lattice point [41]. The basis defines the position of the atoms relative to a lattice point by the vector $\boldsymbol{r_j} = x_j\boldsymbol{a_1} + y_j\boldsymbol{a_2} + z_j\boldsymbol{a_3}$ for each atom j. An ideal crystal structure can be completely described by the three basis vectors $\boldsymbol{a_i}$ and the basis. Since the length and direction of $\boldsymbol{a_i}$ can be chosen freely an infinite number of different lattices exist.

In the following some conventions to identify directions and lattice planes in the crystal are given [42][41][43]: Any direction $\boldsymbol{r}$ in the lattice can be written in the basis of the lattice vectors in the way $\boldsymbol{r} = u\boldsymbol{a_1} + v\boldsymbol{a_2} + w\boldsymbol{a_3}$. Therefore a direction in the crystal lattice can be identified by the three factors of the lattice vectors which are written in square brackets [uvw] by convention. Lattice planes have periodic interceptions with the Bravais lattice and are described by *Miller indices* h,k and l. The crystallographic definition of the Miller indices is: if (a_1, a_2, a_3) are multiples of the absolute values of the primitive lattice vectors which describe the interception points of the plane with the three crystal axes then the Miller indices are the smallest integer multiple of the inverse of (a_1, a_2, a_3) [43]. A specific plane is written in round brackets (hkl). A set of planes which are equivalent because of the symmetry of the lattice can be identified by curly brackets {hkl} and a set of equivalent directions by Angle brackets ⟨uvw⟩.

Crystal lattices can be classified by their symmetry. It is always possible to find a set of point symmetry operations which take the lattice into itself. For the three-dimensional space 14 lattice types (Bravais lattices) can be defined by gradually raising their possible symmetry.

It is useful to define the *reciprocal lattice*: The set of all wave vectors $\boldsymbol{G_{hkl}}$ which produce plane waves with period of a given Bravais lattice is the reciprocal lattice for this Bravais lattice [42]:

$$e^{i\boldsymbol{G_{hkl}}(\boldsymbol{r}+\boldsymbol{R})} = e^{i\boldsymbol{G_{hkl}}\cdot\boldsymbol{r}}$$

$$e^{i\boldsymbol{G_{hkl}}\cdot\boldsymbol{R}} = 1$$

where $\boldsymbol{r}$ is arbitrary and $\boldsymbol{R}$ any point of the given Bravais lattice. The primitive lattice vectors $\boldsymbol{b_i}$ of the reciprocal lattice are related to the real lattice in the following way [41]:

$$\boldsymbol{b_1} = 2\pi\frac{\boldsymbol{a_2}\times\boldsymbol{a_3}}{V}$$

$$\boldsymbol{b_2} = 2\pi\frac{\boldsymbol{a_3}\times\boldsymbol{a_1}}{V}$$

$$\boldsymbol{b_3} = 2\pi\frac{\boldsymbol{a_1}\times\boldsymbol{a_2}}{V}$$

which again are vectors of a Bravais lattice. Therefore one can find again a Wigner-Seiz-Cell which is for the reciprocal lattice called first Brillouin-zone. The vector $\boldsymbol{G_{hkl}} = h\boldsymbol{b_1} + k\boldsymbol{b_2} + l\boldsymbol{b_3}$ is perpendicular to the plane (hkl). This can be also used as a definition of the miller indices.

2.4.2 Laue equation

To explain the diffraction of X-Rays by crystals Max von Laue started from the assumption that a crystal is built out of identical microscopic objects, which are placed on a Bravais

lattice as described in the section above (2.4.1). It is assumed that these objects diffract the incident X-Ray radiation in all directions as a spherical scattered waves. The assumption is correct because the wave length of the X-rays is much greater than the dimension of the atoms and the point of observation is far away from the point of scattering [42][40]. A further assumption is elastic scattering and therefore the wavelength λ is the same for the incident and scattered wave. Reflexes from the crystal lattice can be seen in directions where the scattered waves of all atoms interfere constructive.

For the derivation of the condition for constructive interference we look at an incoming radiation from direction $\hat{\boldsymbol{n}}$ with wavelength λ and the wave vector $\boldsymbol{k} = \hat{\boldsymbol{n}} \cdot 2\pi/\lambda$ which is scattered by two atoms with distance d. For a direction $\hat{\boldsymbol{n}}'$ the scattered waves with wave vector $\boldsymbol{k}' = \hat{\boldsymbol{n}}' \cdot 2\pi/\lambda$ interfere constructive if the difference in the path length is an integer multiple m of the wavelength (see Fig. 11)[42]:

$$d\cos\theta + d\cos\theta' = \boldsymbol{d} \cdot (\hat{\boldsymbol{n}} - \hat{\boldsymbol{n}}') = m \cdot \lambda$$

Multiplication with $2\pi/\lambda$ leads to:

$$\boldsymbol{d} \cdot (\boldsymbol{k} - \boldsymbol{k}') = 2\pi m$$

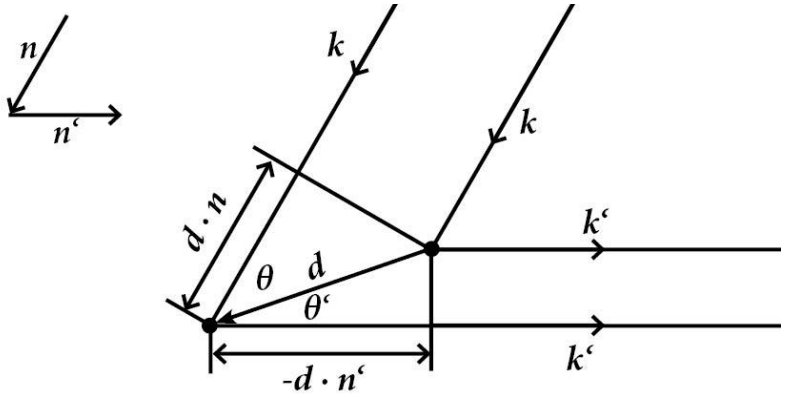


Fig. 11 Laue equation, difference in path length of plane wave scattered by two atoms with distance d. (adapted from reference [42]).

Now it is demanded that this holds for all points of a bravais lattice with any latticevector $\boldsymbol{R}$:

$$\boldsymbol{R} \cdot (\boldsymbol{k} - \boldsymbol{k}') = 2\pi m$$

Which is equivalent to:

$$e^{i(\boldsymbol{k}-\boldsymbol{k}')\cdot\boldsymbol{R}} = 1$$

Comparing this to the definition of the reciprocal lattice (see section 2.4.1) results in a formulation of the *Laue-condition* for constructive interference which says that $\boldsymbol{\Delta k} = \boldsymbol{k} - \boldsymbol{k}'$ has to be equivalent to a reciprocal lattice vector $\boldsymbol{G_{hkl}}$ [42].

Now the Laue-condition can be generalised now for a crystal lattice which has more than one atom in the basis. This is done by using *structure factors* which describes how the interference of the basis atoms *j* lower the intensitiy of the Bragg-reflection for a specific reciprocal lattice vector $\boldsymbol{G_{hkl}}$:

$$S_{hkl} = \sum_j e^{-i\boldsymbol{G_{hkl}}\cdot\boldsymbol{R_j}} f_j^{hkl}$$

Where f_j^{hkl} is the atomic factor determined by the electron density ρ_j of the atom j defined by:

$$f_j^{hkl} = \int \rho_j(r) e^{-i\boldsymbol{G_{hkl}}\cdot\boldsymbol{r}}\, dV$$

The intensity of a peak in a XRD pattern is proportional to the factor $|S_{hkl}|^2$ therefore they can be useful to calculate the crystal-structure of single-crystals out of XRD-patterns. For amorphous structures and less crystalline structures as graphite oxide, the peak intensities and widths depend on other factors like superposition of different crystalline spacing and interstratification (see also section 2.4.4).

2.4.3 Bragg's law

Bragg's law is equivalent to the Laue-condition. It defines a condition in real space which leads to constructive interference of two parallel waves with a certain wavelength (λ) which are diffracted by two crystal-lattice planes separated by certain distance (d) by [44]:

$$n\lambda = 2d\ \sin(\theta)$$

where θ is the Bragg-angle between incoming beam and the crystallographic plane (see **Fig. 12**) and n is a positive integer.

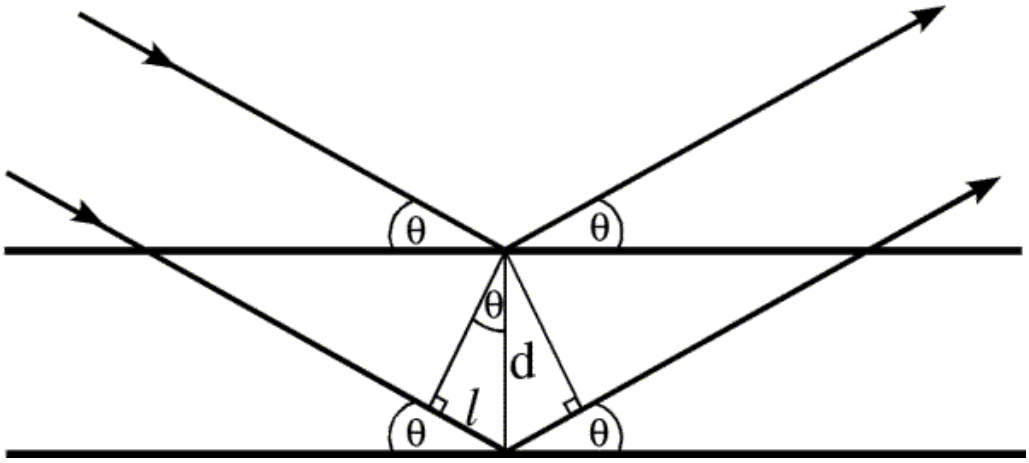


Fig. 12 Bragg's law diagram.

Bragg's law is used for XRD where records the intensity of the diffracted radiation is recorded for different angles. Peaks in the diffracted radiation are measured if the incident beam together with the crystal planes and the detector fulfill Bragg's law. Then the d-spacing for a certain angle can be directly calculated using Bragg's law, if the wavelength of the radiation is known:

$$d = \frac{n\lambda}{2\ \sin(\theta)}$$

2.4.4 Interstratification and Méring's principles

Interstratification is well known and studied on polycrystalline clay-minerals where different layer types with different unit cell parameters are found within one sample [45]. Unlikely to completely amorphous structures peaks can be observed in the XRD patterns.

These peaks are not a superposition of different peaks, but can be explained by a migration of the maximum of the interference function due to the interstratification [46]: For a mixture of two different layer types the peak of the interstratified material appears to be between the positions of the two single-crystalline materials (see Fig. 13). According to the second Méring's principle the peak position of mixed-layer structures show a linear dependence of the proportions of the two layer-types A and B,

$$W_A = \frac{y}{x + y}$$

where W_A is the proportion of layer-type A in the mixed sample and x and y are the distances between the node of the mixed-layer structure and the nearest l_A and l_B nodes of the pristine materials. Furthermore this means that the higher order peaks appear in a nonrational series in the refraction pattern.

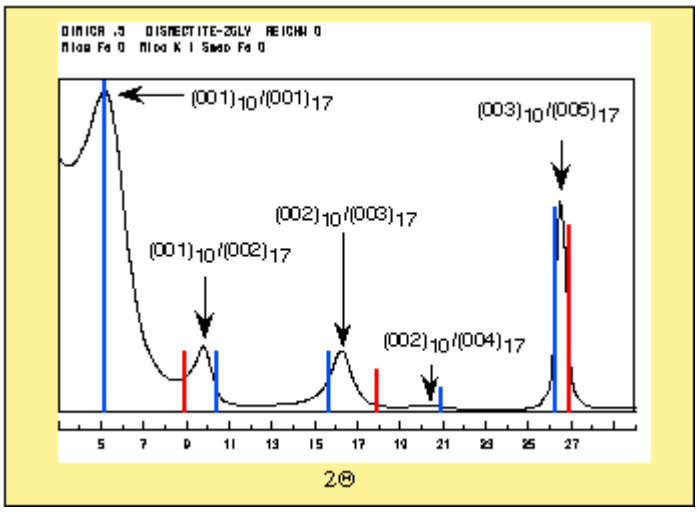


Fig. 13 Example XRD Diffraction pattern of an interstratified clay mineral with two components. The blue and red lines mark the reflections of the pristine components (figure from ref. [45]).

Similar effects seem to appear when for example studying hydrated GO [15] where the peak position does not fit to a discrete number of intercalated monolayers of water. Interstratification makes a detailed interpretation of the XRD patterns more difficult since one can have interstratification not just from two but from more different inter-layer distances.

2.4.5 Radiation from X-ray tubes

In the vacuum in X-ray tubes electrons are accelerated in an electric field and hit then an electrode. When electrons hit the electrode two kinds of radiations are emitted [47]: The radiation due to acceleration when an electron is stopped by the atomic nuclei of the electrode surface. This radiation has a continuous spectrum. The radiation mainly used for monochromatic XRD is called characteristic radiation and corresponds to the transition-energy of an inner-electron to a lower energy-level. This happens if a K-electron is kicked out by the X-ray radiation and then an electron from an upper electron shell turns to fill the empty K-shell.

2.4.6 Synchrotron radiation for XRD

In a synchrotron the X-ray radiation is emitted by relativistic electrons which are guided and accelerated by a magnetic field [47]. Since the electrons are ultra-relativistic the radiation power pattern changes from a normal dipole pattern to a narrow cone in tangential direction of the electron trajectory. This narrow beam with high intensity can be used for XRD.

The spectrum of the radiation emitted by the electrons forced on a circular orbit is described by the following formula (see Fig. 14):

$$\frac{dp}{d\omega} = \frac{P_{tot}}{\omega_c} S\left(\frac{\omega}{\omega_c}\right)$$

where S is the universal function of synchrotron radiation and ω_c the characteristic frequency which is given by

$$\omega_c = \frac{2\, c\, \gamma^3}{2\rho}$$

where ρ is the bending radius and c the speed of light and $\gamma = 1/\sqrt{1-(v/c)^2}$.

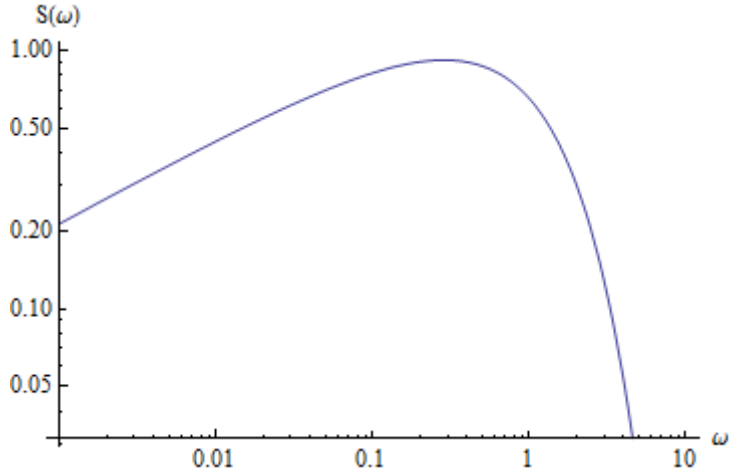


Fig. 14 Arbitrary spectrum of Synchrotron radiation with $\omega_c = 1$.

Instead of bending magnets with a homogenous permanent magnetic field and fixed bending radius ρ Wiggler magnets and Undulators are used for deflect the electrons periodically in space and produce a spectrum with a certain characteristic frequency ω_c [47]. Wigglers cause

larger transverse oscillations of the electrons mainly shift the spectrum and increase the photon flux. Undulators cause weaker periodic deflection which leads to emittance of quasi-monochromatic radiation.

Some of the advantages of Syncrotron radiation over radiation of X-ray tubes are a several orders of magnitudes higher intensity, more uniform spectral distribution and a wide range of wavelength.

2.4.7 Crystal structure of graphite

Also if the structure of graphite oxide and also the graphen oxide membranes is far from perfectly crystalline the lattice structure of pristine graphite can be used to identify the lattice planes and directions. Graphite crystal has a triangular Bravais lattice (also called hexagonal lattice [41]) with a unit-cell consisting of four atoms A, B A' and B' [42]: The triangular lattice is defined such that $a = a_1 = a_2$, $a_3 = arb.$, $\alpha = \beta = 90°$ and $\gamma = 120°$ [48]. Relative to the atom A the other basis atoms have the following positions (see Fig. 15) [49]: atom B: $-\frac{1}{3}\boldsymbol{a_1} + \frac{2}{3}\boldsymbol{a_2}$, atom A:' $\frac{1}{2}\boldsymbol{a_3}$ and B': $-\frac{1}{3}\boldsymbol{a_1} - \frac{2}{3}\boldsymbol{a_2} + \frac{1}{2}\boldsymbol{a_3}$. The basis atoms A and B together form a honeycomb lattice in the (001) plane with a nearest neighbour distance of $\delta = \left|\frac{1}{3}\boldsymbol{a_1} + \frac{2}{3}\boldsymbol{a_2}\right|$. (see Fig. 15 (A)). The atom A' and B' form honeycomb lattice parallel to (001) with a distance to the (001) plane of $d = \frac{1}{2}|\boldsymbol{a_3}|$.

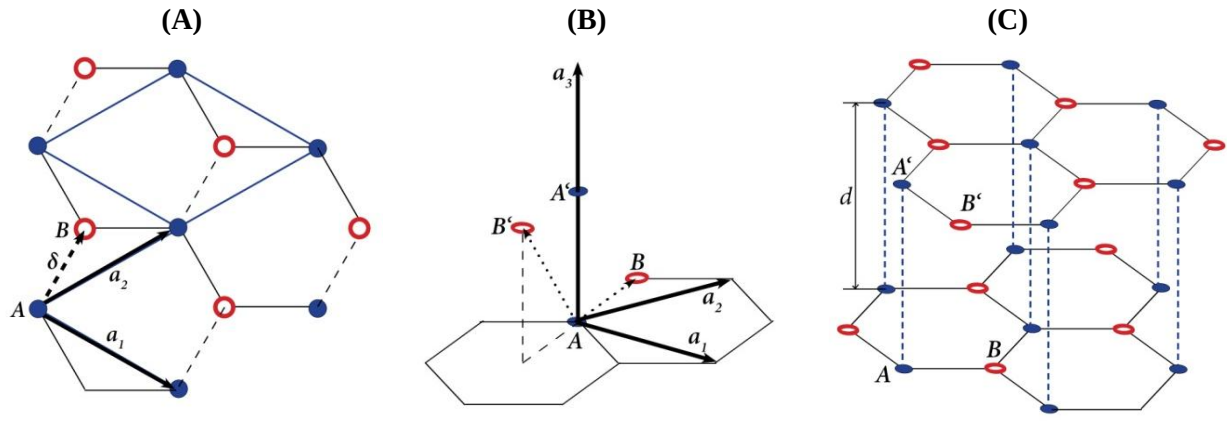


Fig. 15 Lattice structure of graphite. Blue discs mark basis atoms A and A', red circles the basis atoms B and B'. **(A)** Lattice in the (001)-plane, blue lines draw the Bravais lattice in the (001) plane. **(B)** Atoms of the unit cell and lattice vectors $\boldsymbol{a_i}$. **(C)** Illustrations of the parallel honeycomb lattices with distance $d = \frac{1}{2}|\boldsymbol{a_3}|$. (Figures adapted from reference [49]).

The parameters of the hexagonal Bravais lattice for Graphite are the following [50], [49]:

$a = a_1 = 2.46$ Å

$c = a_3 = 6.71$ Å

The nearest neighbour distances are [49]:

In the (001) plane: $\delta = 1.42$ Å

In the (110) plane: $d = \frac{c}{2} = 3.35$ Å

Also a rhombohedral form of graphite with a 3 layer ABC stacking is observed less frequently [49].

The structure factor of graphite is (where hkl are miller indices) [49]:

$$S_{hkl} = \left[1 + e^{-i\frac{2\pi}{3}(2h-k)}\right] \cdot \left[1 + e^{-i\pi l}\right]$$

This means there are no reflections form the planes with odd l because the structure factor of graphite becomes zero($S_{hkl} = 0$) if the miller index l is odd.

In Fig. 16 a XRD pattern of graphite powder is shown. The differences in intensity of the different peaks can be seen clearly. The (003) and (005) peaks are not visible because the structure factor becomes zero for them.

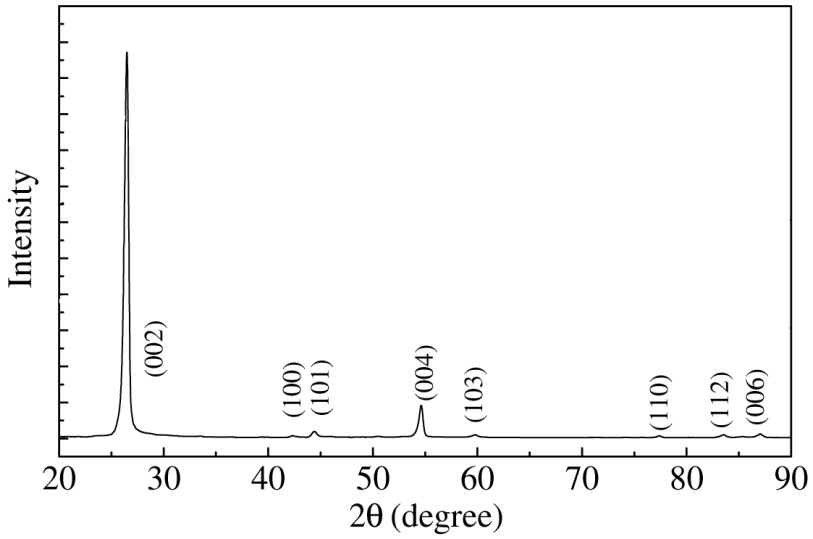


Fig. 16 XRD pattern of graphite (figure reference [51]).

In Fig. 17 XRD patterns of GO and pristine graphite are compared. One can see the narrow (002) peak of graphite compared to the broad (001) peaks of the basal planes of the graphite oxide which are less crystalline.

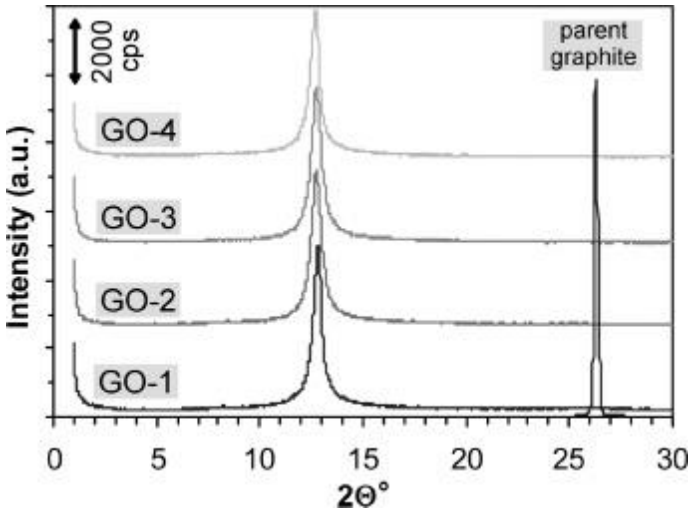


Fig. 17 XRD Pattern of GO prepeared by Brodie method with different degrees of oxidation (GO-1-4) compared with the pattern of pristine graphite (parent graphite) (figure reference [10]).

2.4.8 X-Ray Diffraction geometries

A detailed overview over the classification of experimental diffraction geometries can be found in reference [52]. To stimulate different bragg reflections (fulfil the Bragg-equation) XRD-setups use either a X-ray beam with continuum of wavelengths (for example Laue method) or a monochromatic X-ray beam together with a setup for rotation of the sample (moving-crystal-methods) or a powder-sample with randomly orientated crystals (powder-methods). Geometries can also be divided in reflection, transmission and Seemann-Bohlin geometries (see Fig. 18). For reflection geometry the lattice planes need to be about parallel and for transmission perpendicular to the sample surface.

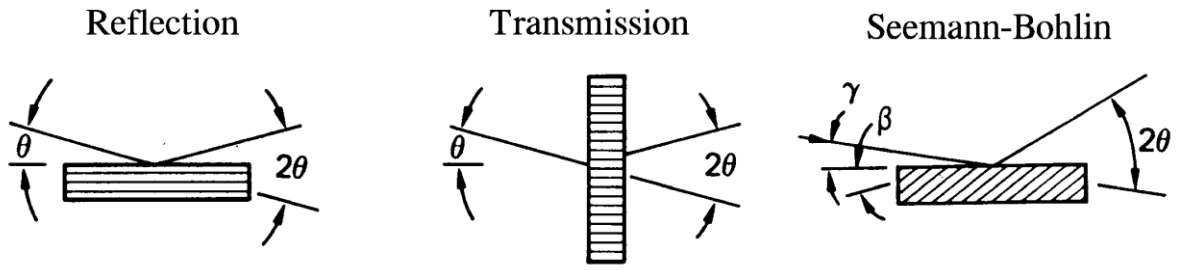


Fig. 18 Transmission vs. reflection geometry. The hatching in the sample indicates the direction of the crystal-lattice planes.

2.4.9 X-Ray Diffractometer Siemens D5000

For the measurements presented below the X-Ray diffractometer Siemens D5000 with CuKα with an average wavelength of $\lambda = 1.5418$ Å was used. The $CuK\alpha_1$ $CuK\alpha_2$ lines can be averaged at low angles because the error $\Delta\theta$ is proportional to $\tan\Theta$:

$$\Delta\theta = \frac{\delta\lambda}{\lambda}\tan\Theta$$

The 2-circle diffractometer with Bragg-Brentano focusing geometry was operated in θ-2θ mode where the x-ray tube is fixed and the sample holder moves at ½ of the angular speed of

the detector to maintain the θ-2θ geometry (see Fig. 19) [39]. For measurements of the [001] d-spacing the membrane was placed on the sample holder such that the (001) planes are in parallel to the sample holder.

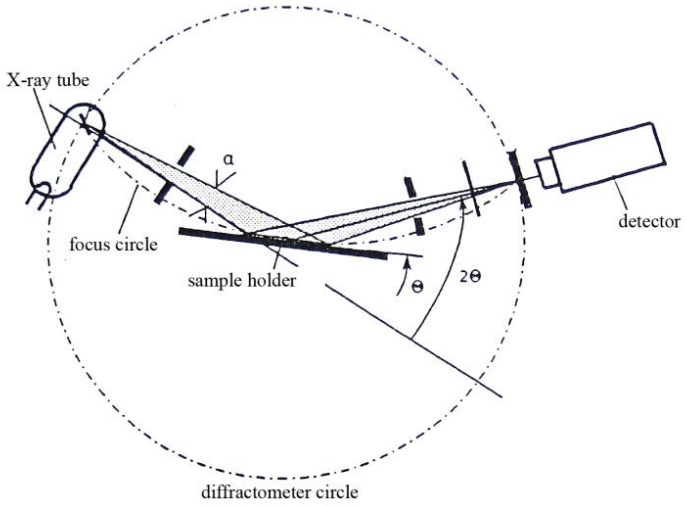


Fig. 19 Reflection geometry in a 2-circle diffractometer (figure adapted from reference [39]).

The peaks of the XRD-patterns were fitted by Voigt profiles (convolution of gaussian and lorentzian profile) with the software Peakfit4. The resulting 2θ-angle was then used to calculate the d-spacing.

The error for the d-spacing Δd which follows out of a error of the Bragg-angle $\Delta\theta$ can be calculated with standard error propagation calculation in first order:

$$|\Delta d| = \left|\frac{\partial d}{\partial \theta}\right| \cdot |\Delta\theta| = \left|-\frac{n\lambda}{2\ \sin(\theta)^2}\cos\theta\right| \cdot |\Delta\theta| = \mathrm{d} \cdot |\Delta\theta| \cdot |\cot\theta|$$

Previous Experiments where silicon was used for calibration showed that the uncertainty $\Delta\theta$ is for $\theta = 9$ deg are about $\Delta\theta$ =0.17 deg. This leads with $\lambda = 1.5418$ Å to an error for d-spacing of $\Delta d = 0.13$ Å. This error estimation was applied for all results which are in the range of θ =6 to 12 deg. The main source of error may is the displacement of the sample and exceeds step size of detector movement (0.03 degrees).

2.4.10 Synchrotron MAX II Beamline 711

Further measurements with membranes immersed in liquids were made at the MAX II Synchrotron in Lund [53]: The X-Ray at Beamline 711 beam comes from a multipole wiggler with a characteristic wavelength of 4.6 Å. The power of the beam is mostly absorbed by a beryllium window which cuts off all wavelengths greater than 3 Å. Apertures and slits define the beam size and a focusing chromium-platinum-mirror cuts off wavelengths shorter than 0.4 Å. An adjustable Si(111) single crystal serves as monochromator providing wavelengths in a range between approximately 0.8 and 1.5 Å (see Fig. 20).

The experimental setup is a 4-circle diffractometer with kappa geometry, capable of doing both single crystal and powder diffraction using a large area CCD detector.

For recording both powder and membrane samples the setup was operated in a transmission geometry (seeFig. 22). And the resulting diffraction cones where recorded with the large area CCD detector.

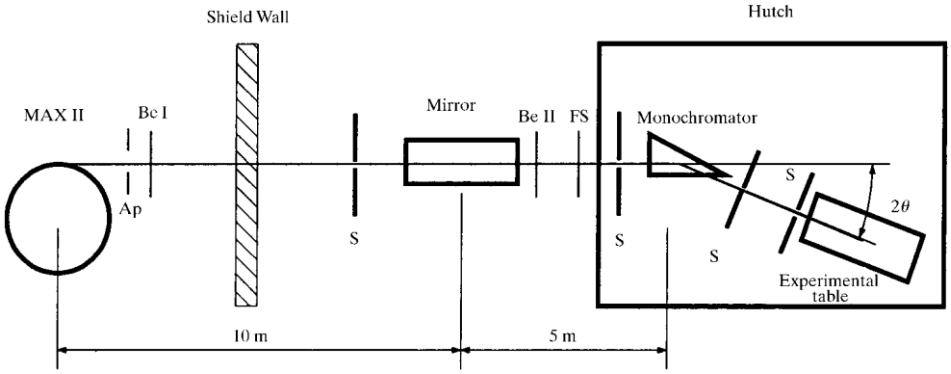


Fig. 20 Layout of beamline 711 at MAX II in Lund "Ap = aperture, Be I = water-cooled Be window, Be II = beryllium window, S = slits, FS = fluorescent screen" (note: the 2θ angle does not refer to the Bragg angle) (figure Ref. [53]).



Fig. 21 Experimental setup at Beamline 711 for XRD measurements.

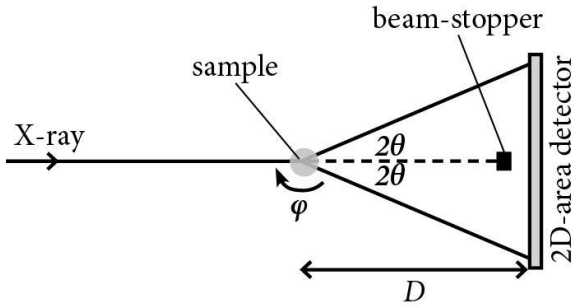


Fig. 22 XRD geometry used for recording patterns of grapheme oxide membrane and powder samples.

The samples were placed in thin glass capillary together with different liquids. The membrane samples were curled to get as many different orientations of the membrane structure as possible. The capillary was then put in the sample holder and rotated around the φ axis for aligning the (001) planes of a membrane piece to fulfil the Laue condition and get a good refraction pattern. For our experiments a wavelength of about 0.99 Å was used and calibrated using a LaB6 standard. The 2D patterns were integrated using Fit2D and PeakFit was used to fit the resulting 1D patterns.

3 Results and discussion

3.1 Synthesis

3.1.1 Graphene oxide Solutions

First step of synthesis is to disperse graphite oxide powder on single sheets in solution which is done by sonication/centrifugation treatment. To compare the results of membrane synthesis the concentrations of the saturated solutions were measured.

Three H-GO solutions were tested which gave the results between 0.6±0.1 and 0.7±0.07 mg/ml after centrifugation (60min at 8000RPM). One H-GO solution was centrifuged for longer time (110min at 8000RPM), which resulted in small decrease of concentration to 0.5±0.2 mg/ml.

Two measurements of a B-GO solution before and after prolonged centrifugation gave a concentration of 1.3±0.2 and 0.9±0.2 mg/ml respectively.

For H-GO further centrifugation and longer storing of the solution did not lead to more visible precipitate, while for B-GO more precipitate could be seen after prolonged centrifugation.

To test the solubility of the precipitate after centrifugation the solution was separated from the precipitate and for H-GO more water and for B-GO more NaOH solution was added to the precipitate. This new solutions were sonicated and centrifuged like the solutions before. For H-GO the solution had a similar colour like the original solution, but for B-GO after centrifugation the NaOH solution was just slightly yellow coloured.

It can be summarised that the H-GO solution is more stable then the B-GO solution, but the B-GO solution has a higher concentration.

3.1.2 Deposition of membranes using different precursory GO Solutions

The Deposition of the membranes is mainly affected by vacuum (regulated by precise valve), type of precursor GO solution, dilution of solutions and of course amount of solution. To evaluate effects of these parameters several experiment sets were performed. The main results are following:

Most of the membranes grown out of SL-H-GO solutions had a flaky macrostructure (see **Fig. 23**). Only when the filter holder was not closed firmly enough some solution could bypass the filter and the resulting membrane was homogenous. This effect is assigned to graphene oxide sheets agglomeration into some flakes in solution.

Membranes grown out of H-GO solutions are in general more homogenous and show different grades of transparencies depending on thicknesses (proportional to amount of solution used) (see **Fig. 24**). A flaky structure like for SL-H-GO membranes was never observed.

B-GO membranes are even more homogenous and show a more yellowish colour. Furthermore they are much more transparent then H-GO membranes grown with the same amount of solution, even though the solutions have a higher concentration.

The length of time needed for growing the membranes was evaluated approximately. For 4ml of saturated H-GO it took roughly one hour to grow the membrane (as stated above the membranes grown that fast, were not very homogenous). For the same amount of B-GO solution it took between 4 and 7 hours. The valve position (vacuum quality) was approximately the same for both experiments.

The reason for the flaky macrostructure of the SL-H-GO might be the addition of some unknown impurities added to in the synthesis process of the pristine material for better dispersion. It seems likely that the GO flakes already formed macroscopic flakes in the solution which were deposited in the end of the filtering process. If the solution bypassed the filter these macroscopic flakes could be washed away. Exact reasons for poor performance of SL-H-GO applied for membranes deposition was not investigated and no further experiments with this material/membranes were performed.

The longer growing time for B-GO membranes is the result of lower permeability for water of the B-GO membranes. This is also confirmed by vapour permeation experiments later (section 3.5).

In conclusion, SL-H-GO seems not suitable for growing homogenous membranes, the H-GO membranes are less transparent then the B-GO membranes and the growing-time is longer for B-GO membranes.

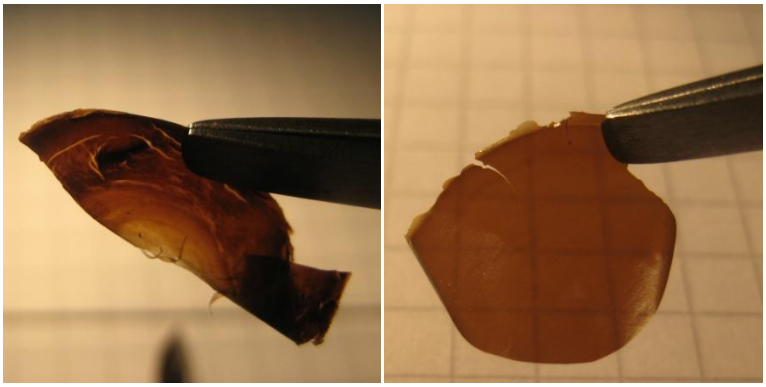


Fig. 23 SL-H-GO membranes: typical inhomogeneous flaky result (left) and one more homogenous result if some of the solution can bypass the filter (right).

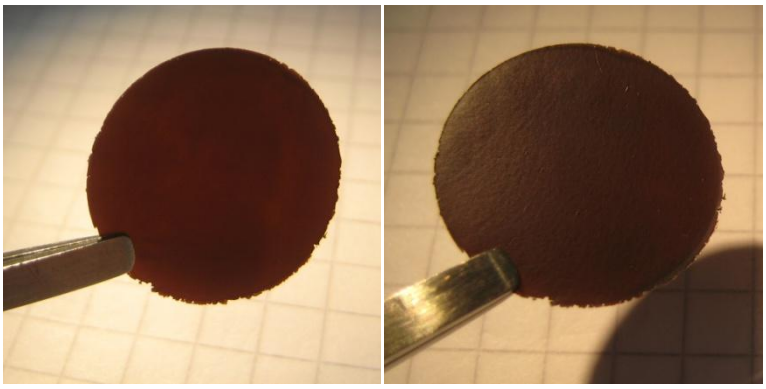
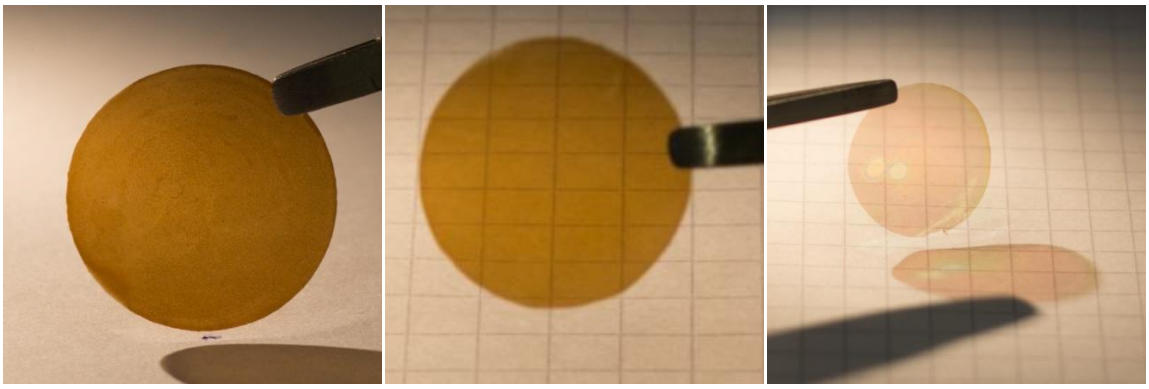


Fig. 24 H-GO membranes: two typical quite opaque specimens


Fig. 25 B-GO membranes: two typical very transparent specimens (left) and one very thin (right)

3.2 SEM imaging

By using a Scanning Electron Microscope (SEM), the structure of the B-GO and H-GO membranes was made visible. The SEM micrographs were recorded by Per Hörstedt.

The image of the cross section of the B-GO membrane shows that the membrane is about 2 µm thick (see Fig. 26 (A)). The membrane is built up out of about 50 lamellas. The ends of the lamellas seem to curl a little bit, so the actual thickness of the lamellas cannot be measured out of this SEM pictures, but a maximum thickness of 30-60nm can be estimated. According to the XRD measurements (see section 3.3) this maximum lamella thickness equates with about 40-85 graphene-oxide layers. The lamellas are not completely plane, but slightly rippled.

SEM Images of the surface also show a wrinkled structure. On the side where the membrane touched the filter when growing, aluminium particles can be seen.

The SEM micrographs in Fig. 29 and Fig. 30 show an H-GO membrane which has a thickness of about 1.5 µm. The H-GO membrane has a more disordered and wrinkled structure then the B-GO membrane. The thickness of the lamellas is about 25 nm. This corresponds to about 30 layers of H-GO flakes.

Again a difference between H-GO and B-GO membranes can be seen. As mentioned in section 1.2 the B-GO seems to have a more crystalline structure then the H-GO which might also be the reason for the more wrinkled structure of the lamellas.

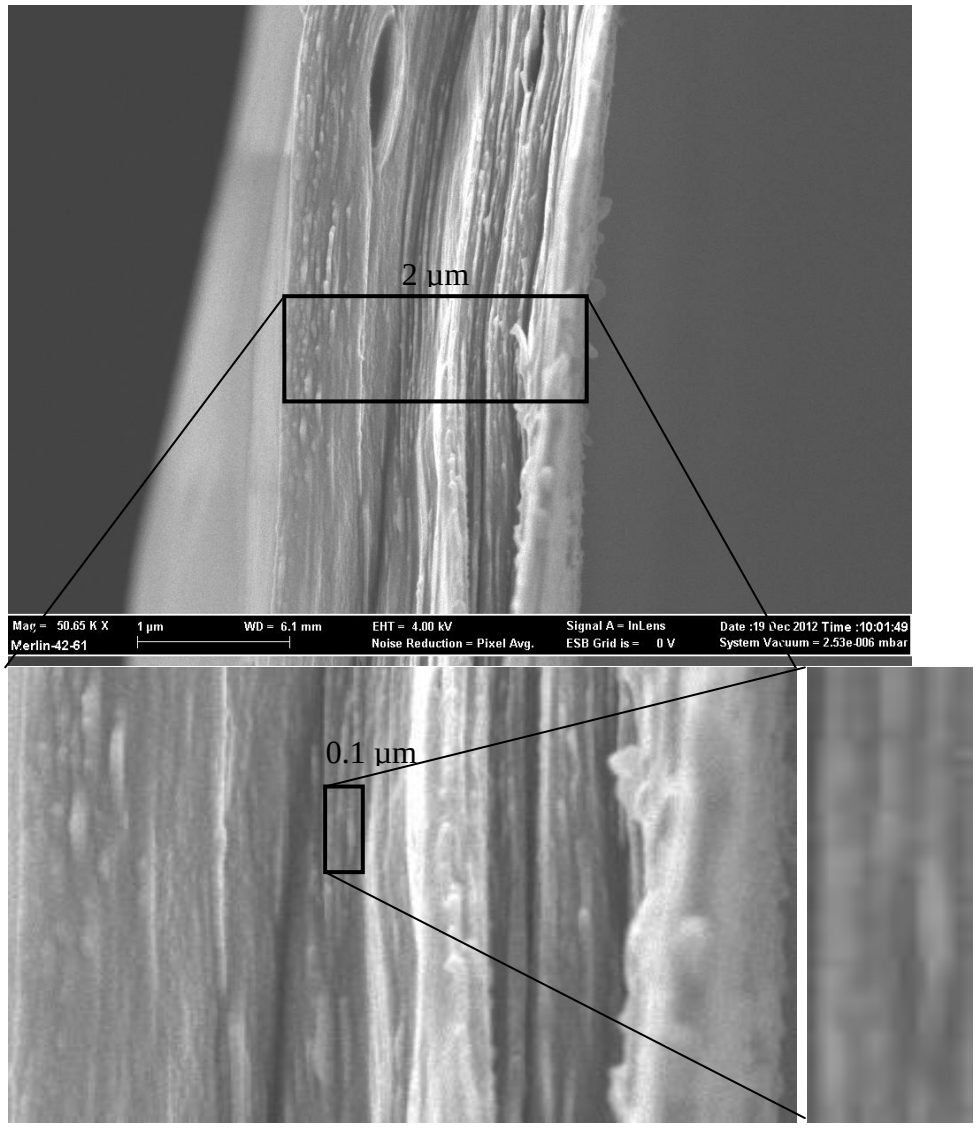


Fig. 26 SEM micrograph of B-GO membrane cross section. (Recored by Per Hörstedt)

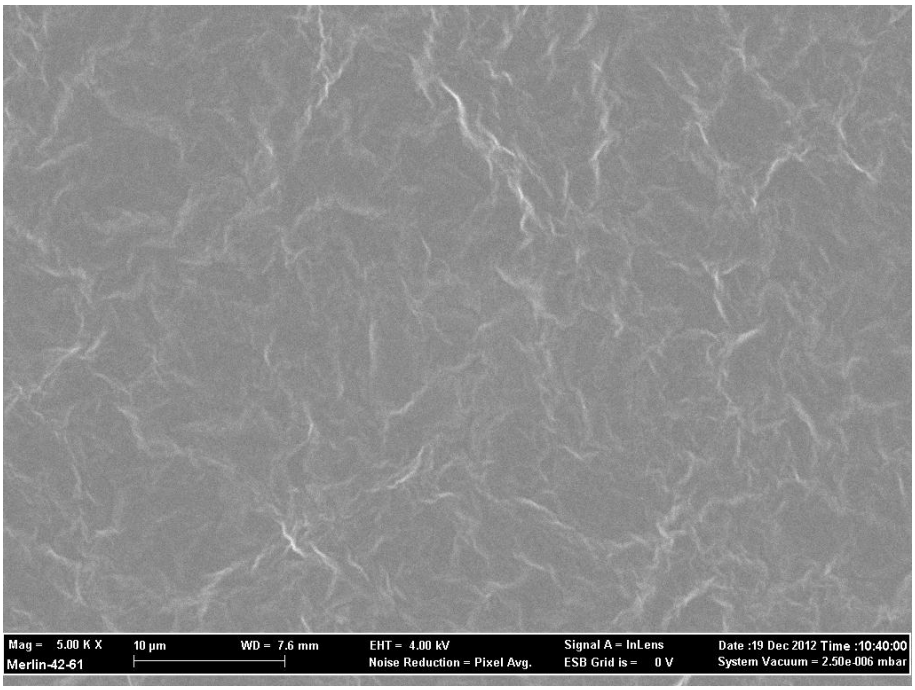


Fig. 27 SEM Picture of the surface of the B-GO membrane. One can see that the surface is not plane, but wrinkled. (Recored by Per Hörstedt)

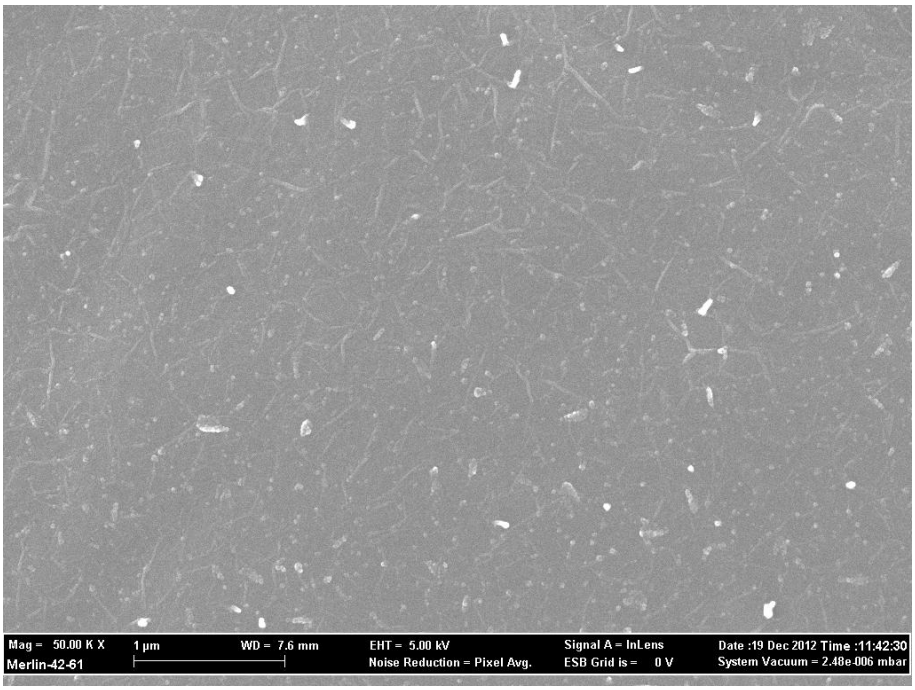


Fig. 28 SEM Picture of the surface of the B-GO membrane of the side which was the filter. One can see the contamination with aluminum. (Recored by Per Hörstedt)

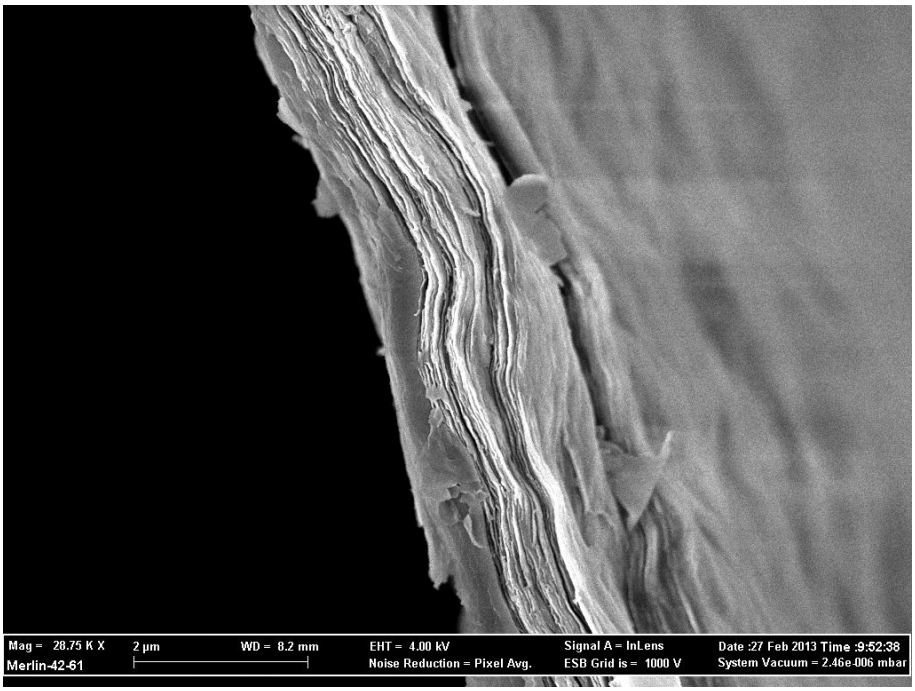


Fig. 29 SEM micrograph of H-GO membrane cross section. (Recored by Per Hörstedt)

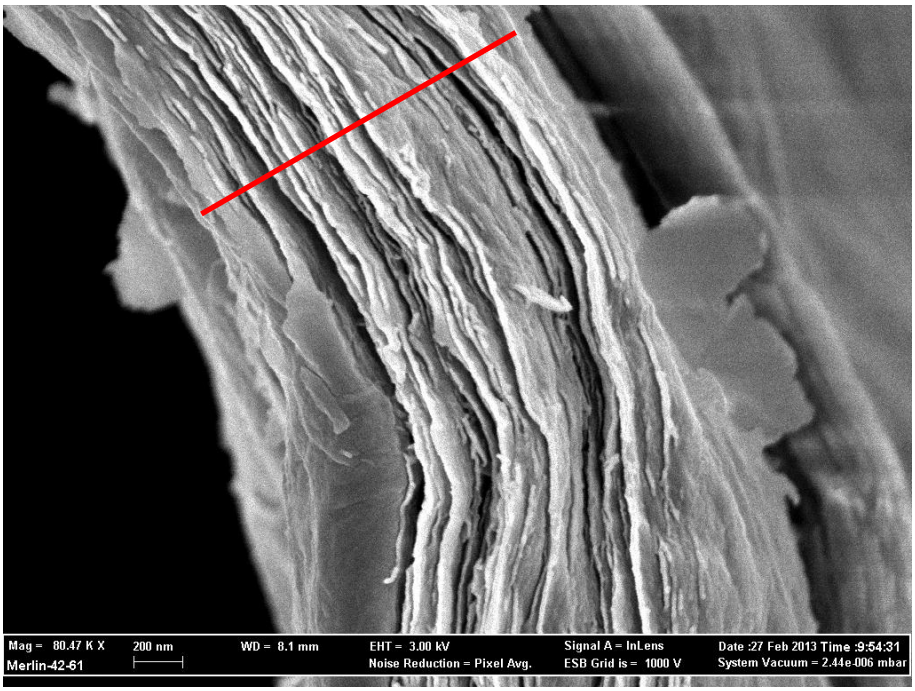


Fig. 30 SEM micrograph of H-GO membrane cross section detail. The red line is 1.5 µm. (Recored by Per Hörstedt)

3.3 XRD analysis

One Important property of GO membranes is the layered structure formed by individual graphene oxide sheets of irregular shapes and sizes. The packing order of GO sheets in the membranes is affected by various parameters e.g. by method of precursor GO synthesis or amount of intercalated water for example. The distance between the layers ((001) d-spacing) can be measured using XRD.

Fig. 31 shows typical XRD-patterns of one recorded from SL-H-GO, H-GO and B-GO membrane each. One can see for SL-H-GO membrane a peak near to 10 deg and for H-GO one near to 11.5 deg. For B-GO a very sharp peak near to 7.1 Å (12.5 deg) and one further peak near to 3.5 Å (25 deg) is visible. These peaks are interpreted as (001)-reflection and (002)-reflections of the GO. The (002)-peaks for SL-H-GO and H-GO cannot be identified while the (002)-peak of B-GO is clearly visible. Further peaks visible in the pattern of SL-H-GO and H-GO are coming from a foil used to fix the membrane on the sample holder and can be ignored. The (001) d-spacing directly corresponds to distance between graphene oxide layers in GO structure.

The membranes were characterized using XRD patterns recorded usually 2-3 days after synthesis. The results are summarized in Fig. 33 (A,B,C). An average value of 8.8±0.4 Å for SL-H-GO membranes, 8.3±0.2 Å for H-GO membranes and 7.3±0.1 Å for B-GO membranes was calculated for (001) peaks.

The (001) d-spacing of pristine powder of SL-H-GO, H-GO and B-GO was measured as 7.7 Å, 7.18 Å and 6.35 Å respectively [12] (see **Fig. 34**). This is about 1 Å less than the value for the membranes a few days after synthesis.

However, later analyses showed that position of (001) reflection shifts upon longer storage at ambient conditions (see **Fig. 32**). It then gives a similar (001) d-spacing as for pristine powder. Slow decrease of inter-layer spacing of graphite oxide is suggested to be a result of water evaporation. The membrane can be considered as one huge flake of graphite oxide and water is likely to be stronger trapped in the membrane compared to the pristine powder which is composed of micrometer size flakes.

The average FWHM for H-GO is 1.4±0.2 Å and for B-GO 0.4±0.1 Å. However, these less broad peaks of B-GO were also observed for the powder samples [12]. It should also be noted that B-GO membranes are better ordered compared to H-GO.

In conclusion of this section, the GO membranes are found to consist of planar sheets stacked in parallel orientation. The ordering of these sheets is qualitatively similar to the one in pristine graphite oxide powders. However the d-spacing of freshly prepared membranes is slightly higher and decreases slowly under ambient conditions.

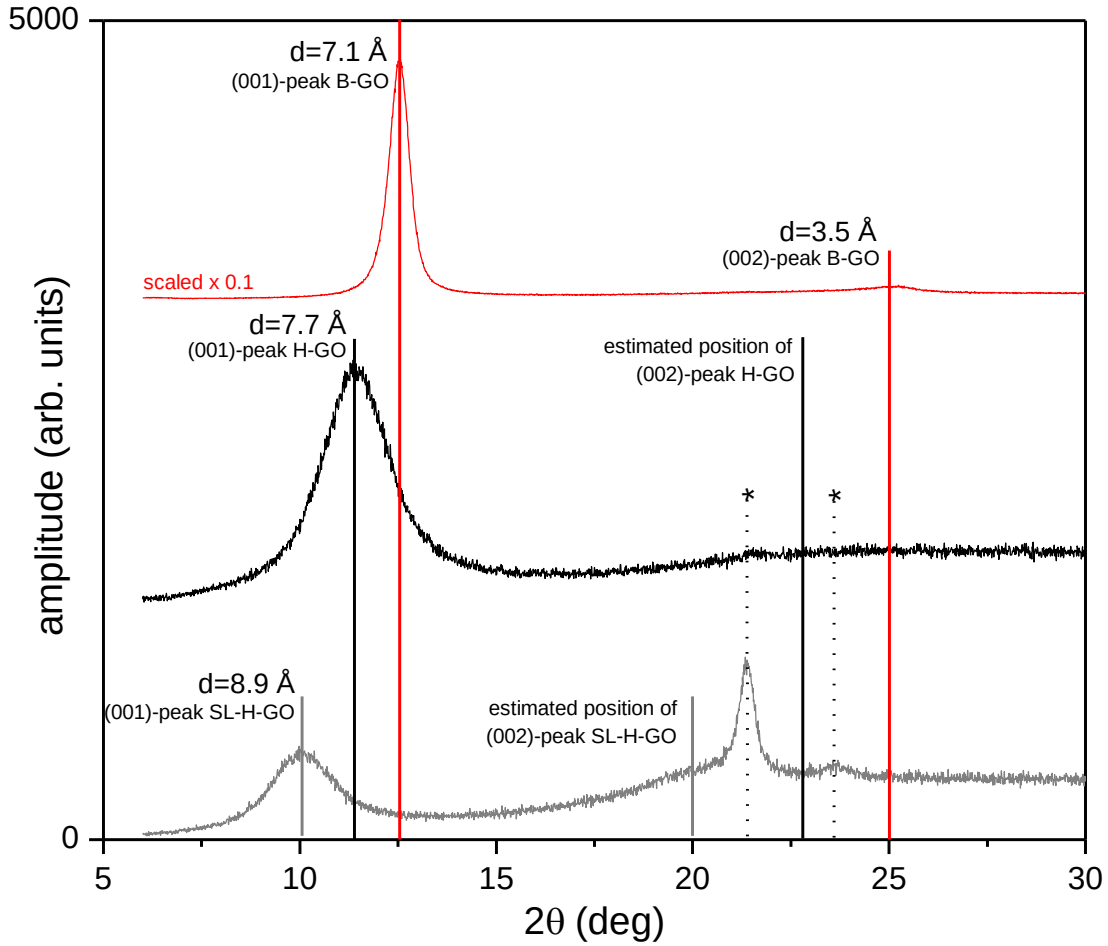


Fig. 31 XRD-pattern of **SL-H-GO** membrane (gray), **H-GO** membrane (black) and **B-GO** membrane (red). The vertical lines mark the peak positions of the first order (001) and second order (002) reflexes. (*) Peaks from the foil which was used to fix the membrane on the sample holder superpose the patterns of the H-GO and SL-HGO membrane.

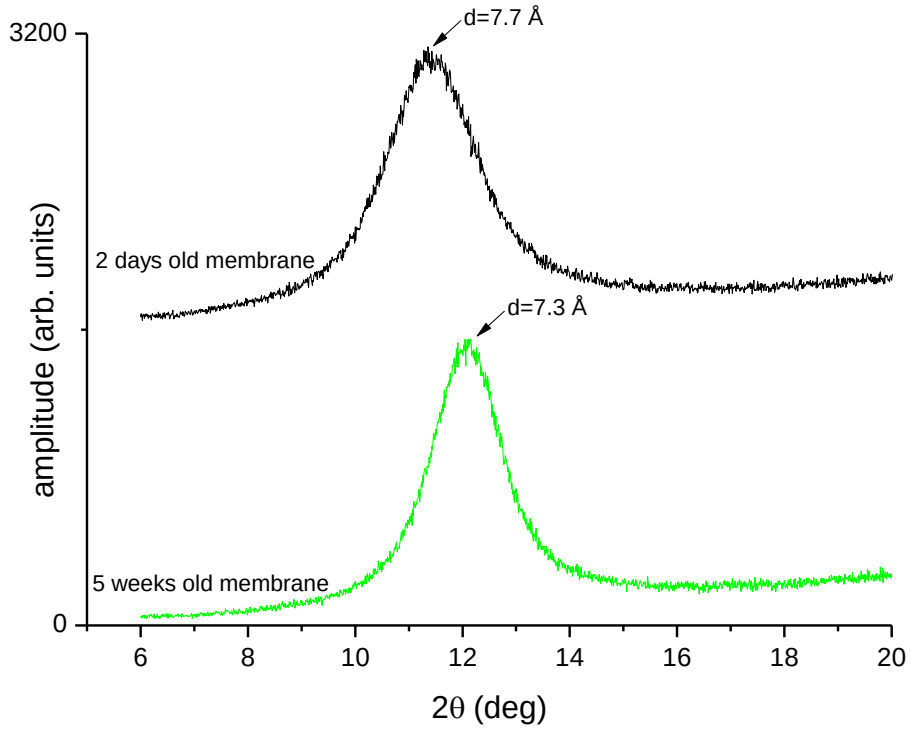
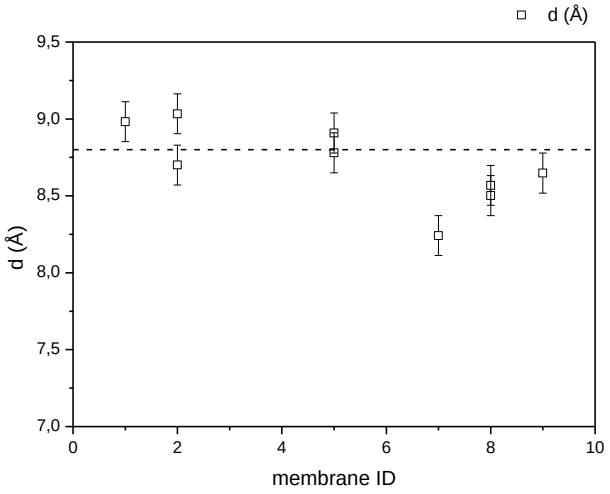
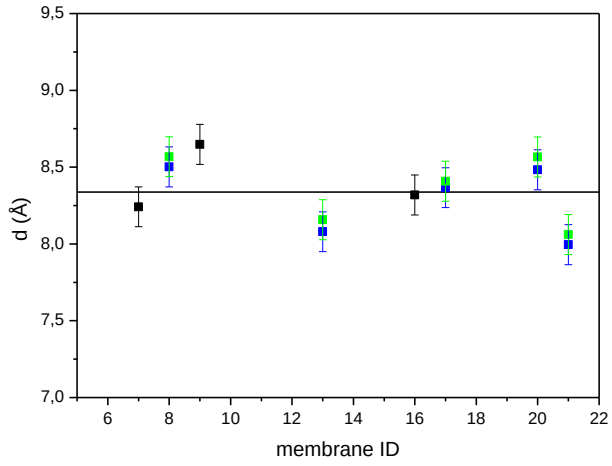


Fig. 32 XRD-pattern of a 2 days old membrane (black) and a 5 week old membrane (green).

(A) SL-H-GO Membrane:



(B) H-GO Membrane:



(C) B-GO Membrane:

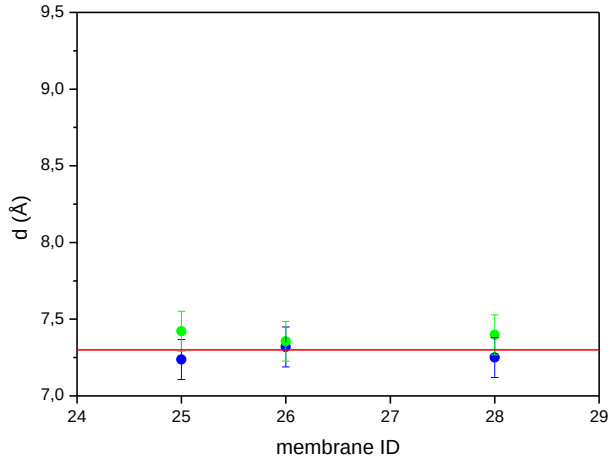


Fig. 33 Overview over d-spacings of various membranes one to three days after synthesis. The membrane ID identifies the membrane for further reference. The colors indicate measurements of the top-side (blue ■,●) and bottom-side (green ■,●) of the same membrane. The horizontal lines indicates the average values for all measurements in a plot. The error bars show the estimated error (see section 2.4).

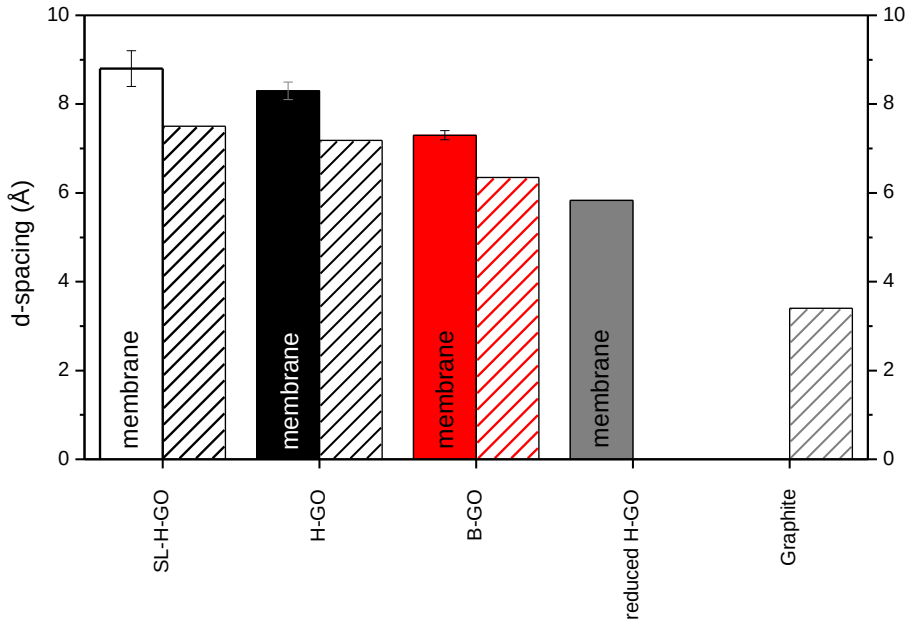


Fig. 34 The solid bars refer to measurements on membranes one to three days after synthesis and the shaded bars to measurements on the basis material. The error-bars indicate the standard deviation of the measurements. The bar for (partly-) reduced H-GO refers to the measurement of the membrane exposed for 4 hours at 145°C.

3.3.1 H-GO Membrane immersed in water

As described in the introduction (section 1.3) GO is very hydrophilic and the inter-layer distance is strongly affected by the amount of water intercalated in the GO. To study the behaviour of GO in membrane form a SL-H-GO membrane was immersed in water.

After immersing a SL-H-GO membrane in water and covering with a foil the (001) d-spacing was measured by XRD. Fitting gives a d-spacing of about 13 Å which is about 5 Å higher compared to "dry" membrane. The expansion of H-GO lattice in liquid water is found to be similar for membrane and powder samples.

The process of membrane de-hydration was studied in experiment with water-saturated sample covered by incompletely sealed plastic foil which allows slow evaporation of water. XRD patterns were continuously recorded until the membrane dried up, see **Fig. 35**. The recording time of one pattern was 25 minutes for first few patterns and 30 minutes for last patterns. Evolution of (001) d-spacing in process of membrane drying is shown in **Fig. 36**.

As it can be seen clearly in Fig. 35, the pattern recorded after 1.5 hours (yellow) does not show of one single sharp peak, but a very broad and asymmetric profile which might be the overlap of multiple peaks. Also the other peaks show some asymmetry. Therefore the d-spacing calculated out of the result of fitting a single peak in the pattern, does not reflect an exact d-spacing of a certain crystalline compound, but seems to be the result of the combination of multiple similar d-spacings or interstratification (see section 1.2 and 2.4.10).

The de-hydration of GO membranes starts when excess of liquid water is evaporated form the sample and become slower with time and finally the d-spacing stabilizes at approximately

8.5Å, near to the value of the pristine “dry” membrane, see **Fig. 36**. The kinetic of the drying process would be, of course, much faster if no plastic foil was used.

As stated above, the value of 8.5Å is not final and slowly decreases in process of further air exposure. It takes more than one week until the d-spacing decreases to the one of pristine H-GO powder. It can be concluded that there is some water which is more strongly trapped then compared to (most of) the water in pristine powder.

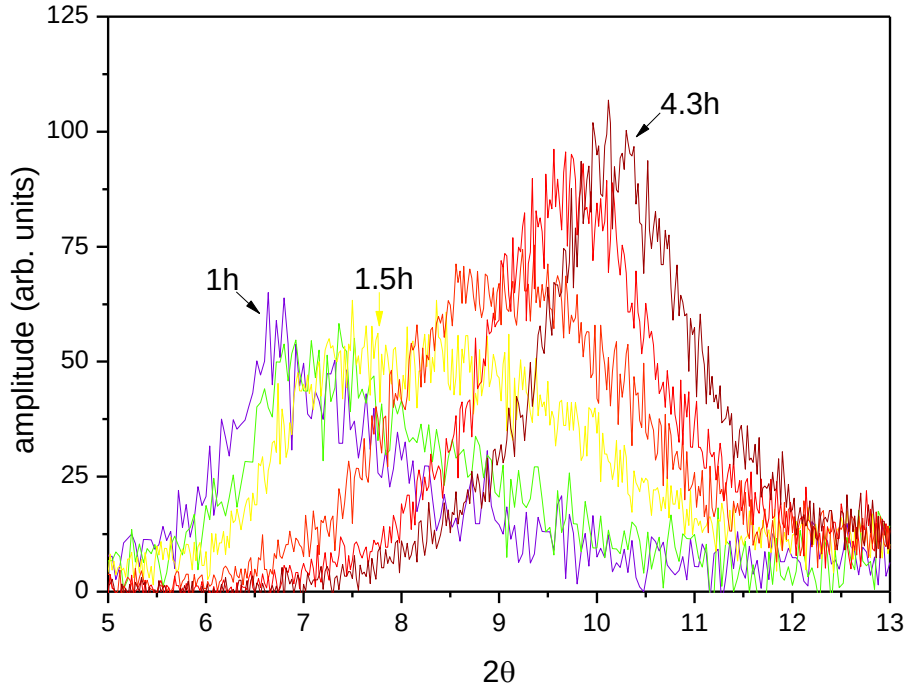


Fig. 35 Time evolution of the XRD-patterns in process of drying starting from wet membrane (violet) to dry membrane (dark red). The background was approximated linearly and subtracted. (Membrane ID: 5, SL-H-GO)

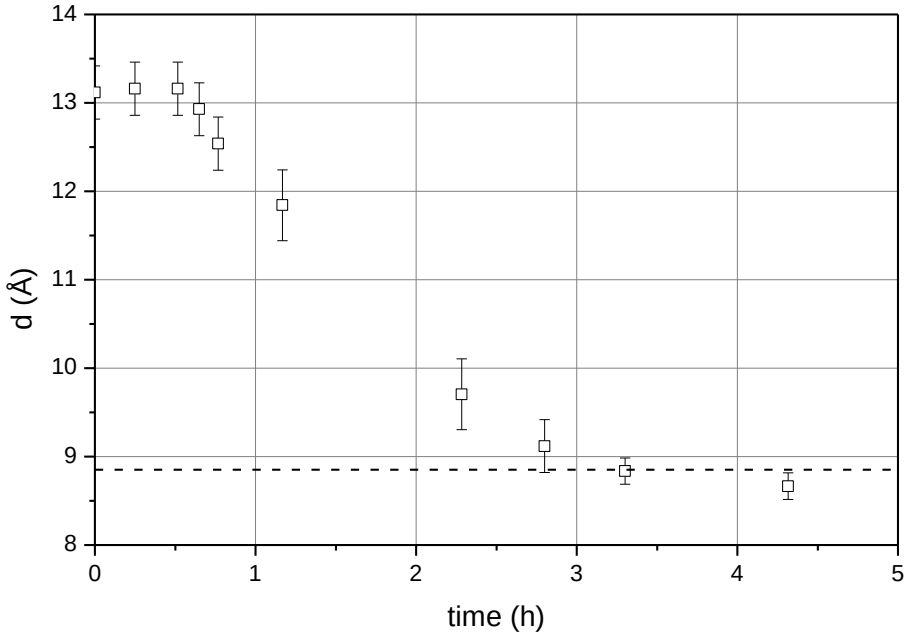


Fig. 36 D-spacing of a Single-Layer-H-GO membrane immersed with water and partly covered by a foil while drying over time (□). The dashed line indicates the d-spacing before it has been immersed with water. The membrane was covered by a foil with small holes so it could dry only slowly. The membrane was grown out of Single-Layer-H-GO solution.

This result is consistent with structural model of membrane as one single flake of graphite oxide. The evaporation of water from graphene oxide inter-layers goes fast for subsurface region of the membrane while those layers which are placed deeper in the micrometer thick membrane are still saturated with water. This results in inhomogeneous hydration of the overall thickness of the membrane and reflected in multiple peaks revealed at this stage of drying by XRD. For GO layers placed deep inside of the membrane water need to diffuse through the network of graphene oxide sheets to reach the surface which explains why the drying process becomes slower with time. The rate of water diffusion to the surface of membrane is also slowed by decrease of inter-layer distance in stronger dried subsurface regions which results in blocking effect and water trapping in the central region of the membranes.

In conclusion of this section interlayer distance of the membranes after hydration increases similar to the one of pristine powder. When the membrane dries up the interlayer spacing decreases to the value of freshly grown membranes within several hours.

3.3.2 Reduced membranes

As it was demonstrated in original study by Nair et al. [4] the permeation of water trough membrane completely vanishes after reduction of graphene oxide. Therefore, some of the H-GO membranes were reduced to verify this effect. Initial experiments with reduction by laser were not successful. The reduction by laser light results in explosion-like modification of membrane flakes and extremely inhomogeneous samples not suitable for permeation tests. Therefore, we tested slow reduction by thermal annealing. The temperature of annealing was selected to be below rapid exfoliation point and as low as possible to allow the reduction but simultaneously not to damage membrane microstructure.

After one hour at 145°C the d-spacing of the membrane was decreased by about 1.5 Å. Further annealing resulted in approximately linear kept decreasing of inter-layer distance at a rate of about 0.2 Å/h (see Fig. 37). The reduction for membrane also correlated with decrease of (001) reflection intensity (see Fig. 38). It could possibly be expected that reduction of GO results at some moment in formation of graphitic phase. However, no additional peaks which could be assigned to graphitic regions could be found in patterns recorded from annealed samples.

Extrapolation of the d-spacing according to observed linear trend back to starting time provides value for d-spacing of about 6.7 Å, which is more similar to the value of 7.2 Å for pristine GO powder rather than the 8 Å of the not reduced membrane. It can be suggested that initial rapid decrease of layers separation is partly due to removal of trapped water, not only reduction of the sample. It is known that graphite oxide absorbs water from humid air and samples exposed to air at ambient conditions are slightly hydrated.

In conclusion of this section, XRD experiments with heated membranes demonstrated that within the first hour of heating the interlayer-distance decreases stronger than in the hours after.

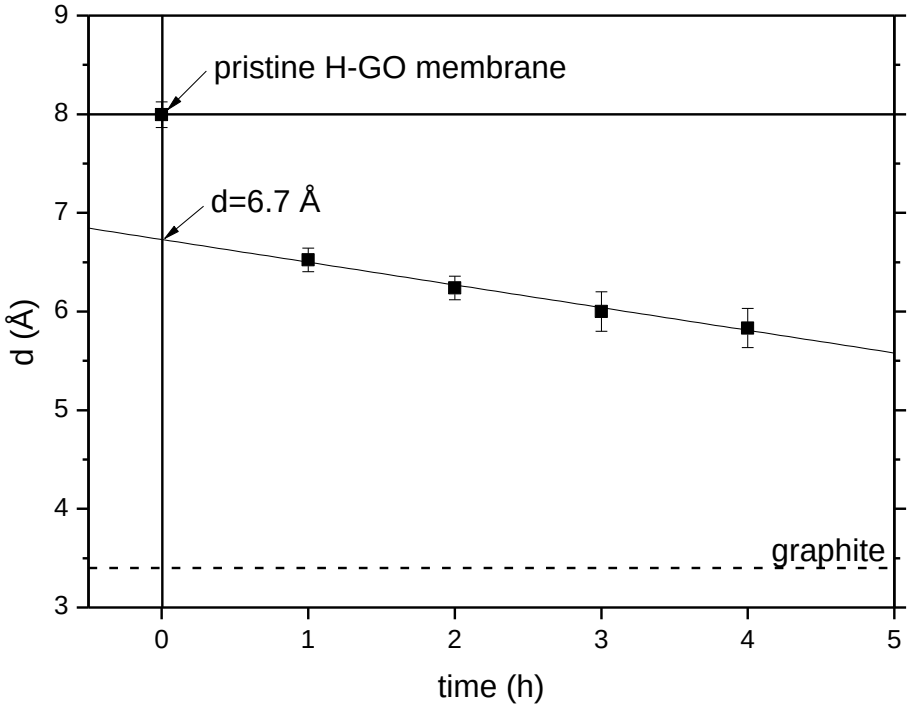


Fig. 37 D-spacing of H-GO membrane versus time of heating at 145°C. The horizontal solid line shows the d-spacing of pristine membrane, the horizontal dashed line shows the d-spacing of graphite.

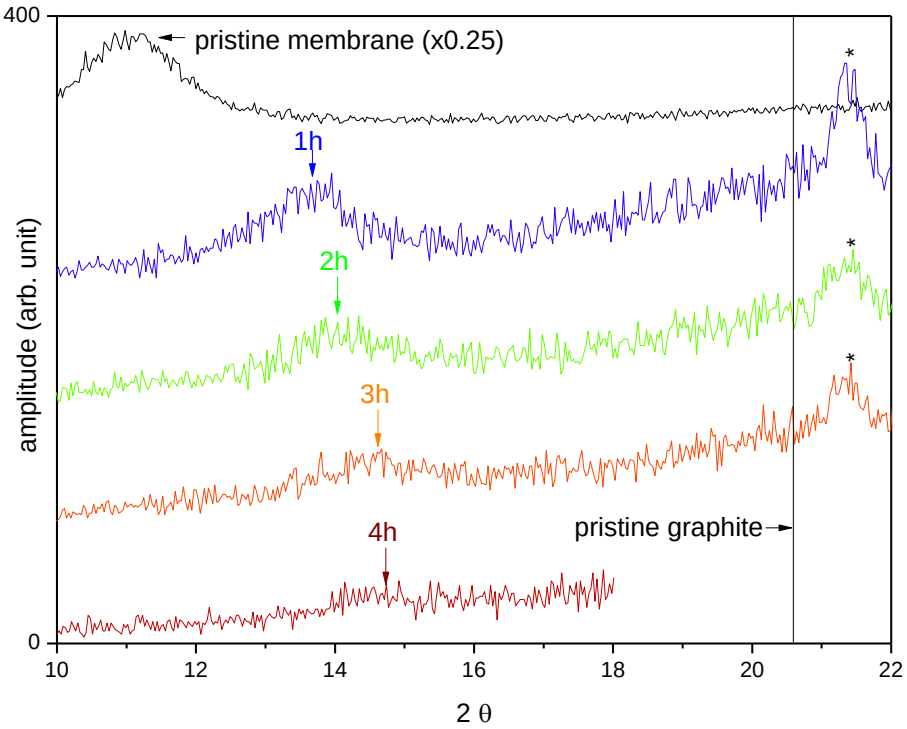


Fig. 38 XRD patterns membrane for different times of heating. Black: pristine membrane, blue: 1h, green: 2h, orange: 3h, brown: 4h heating. The vertical line at 2θ=20.6 deg (≙4.3 Å) marks the angle where a peak of pristine graphite would be expected. The peak of the pristine membrane was scaled down by the factor 0.25 and it was recorded with a bigger piece of the membrane. The marked (*) peaks come from the foil which was used to fix the sample on the sample holder.

3.3.3 Membrane immersed in ethanol

To get a better understanding of the permeability of ethanol a B-GO membrane immersed in ethanol was studied by XRD at the Beamline 711 at the MAXII synchrotron. Because of the high intensity of the X-ray beam also weak peaks can be observed.

The XRD-pattern in Fig. 39 and Fig. 40 shows three peaks. The 2D-Diffraction pattern does not show diffraction rings, but one reflection series in one direction (see also Fig. 41 for H-GO membrane and powder).

The two peaks at an angles of 8.2° and 16.3° can be interpreted as (001) and (002) peaks of the same structural feature with a d-spacing of about 9.1±0.1 Å. This is similar to previous measurements on powder samples immersed in ethanol [20]. The peak at 10.8° (7.0 Å) has the same position as (001) peak of dry B-GO powder.

These results show that there is a difference in intercalation of B-GO in powder and membrane form. While powder immersed in Ethanol is intercalated totally within seconds [20], membranes are only partly intercalated. The membrane was curled in the capillary so that a certain direction of the flakes dominates and only the reflection of this direction exists (see also section 2.4.10). Therefore the absence of complete refraction rings is a result of the parallel alignment of the graphene-oxide flakes in the membrane (see Fig. 41).

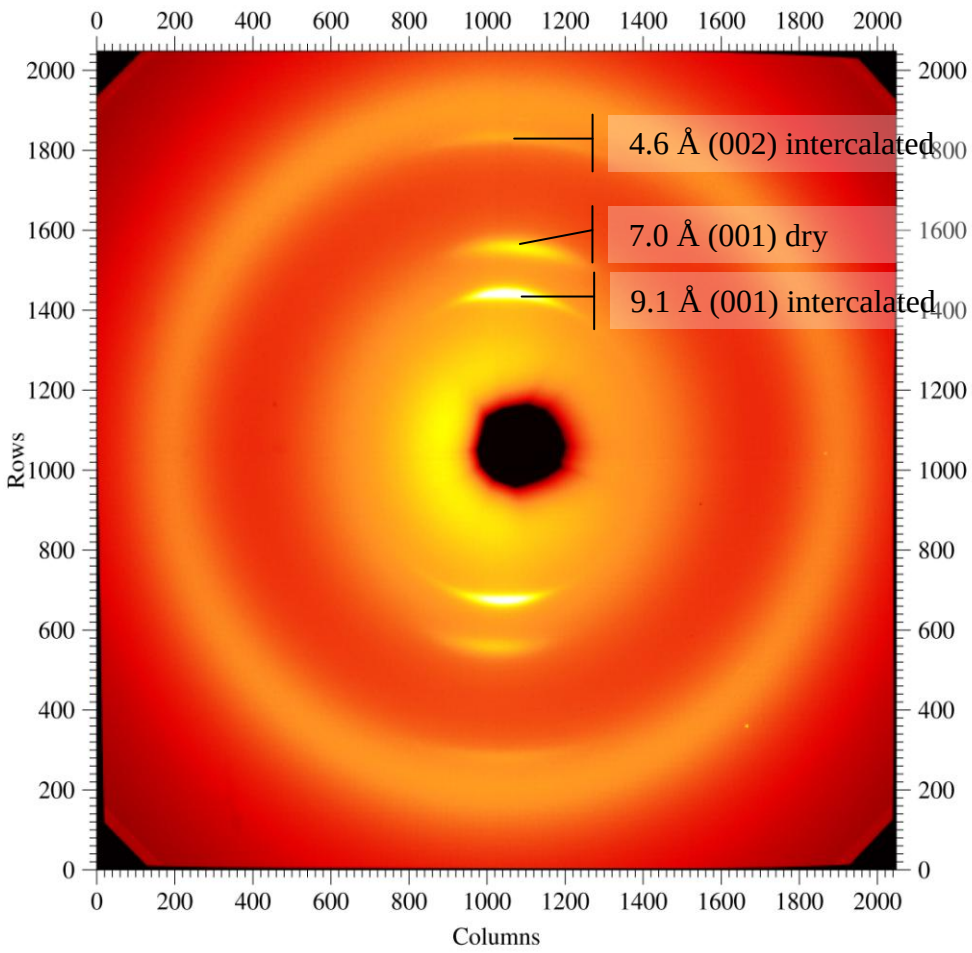


Fig. 39 XRD-pattern of the B-GO membrane recorded with a 2D-detector in transmission geometry.

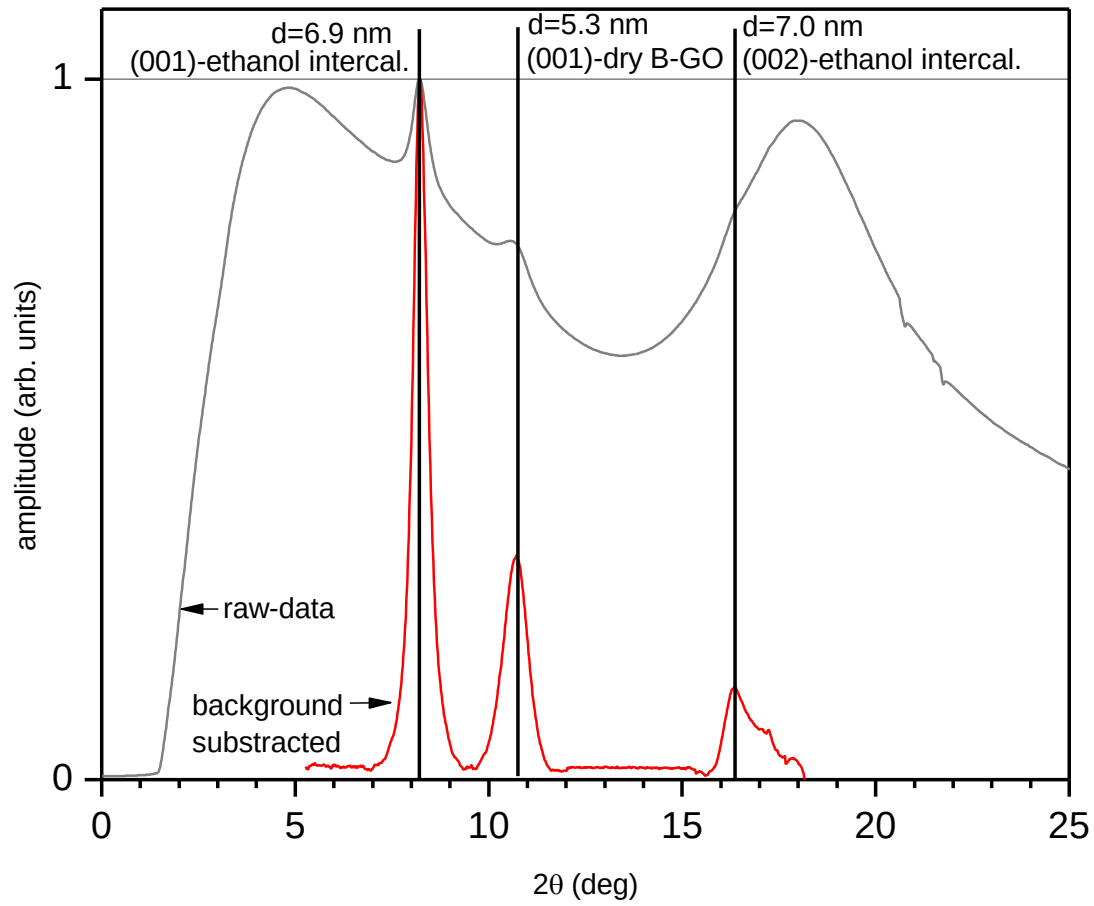


Fig. 40 Integrated XRD-pattern of Fig. 39. The data with background of ethanol is plotted in gray and the data with subtracted background is plotted in red. The amplitude was normalized to 1.

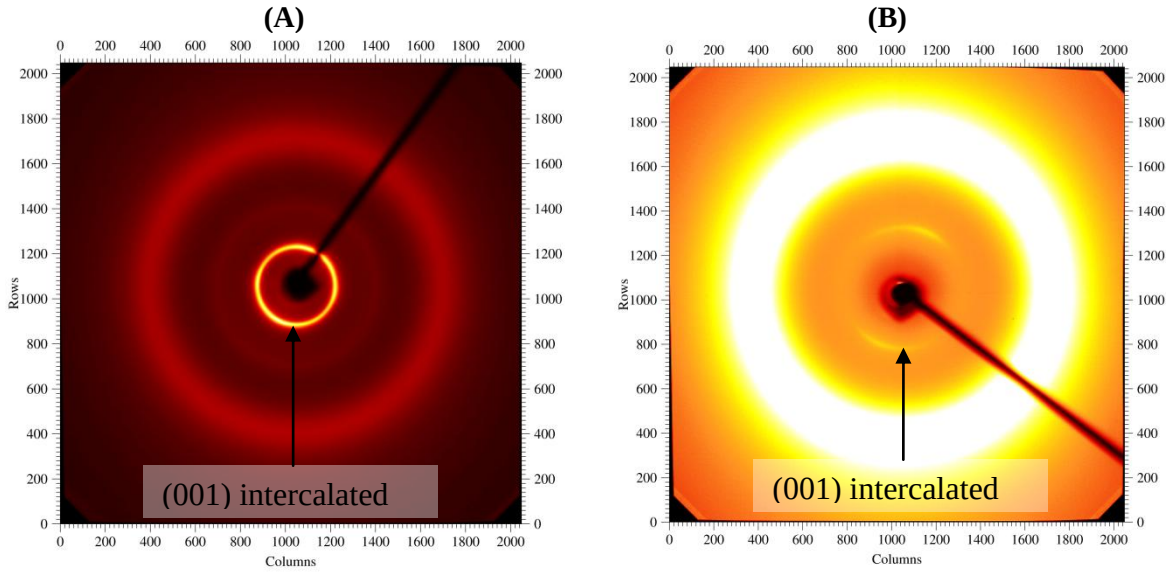


Fig. 41 (A) H-GO Powder immersed in a liquid: the full circle of the (001) reflection is visible. (B) H-GO membrane immersed in a liquid: only partial reflection ring due to parallel alignment of the graphene oxide flakes can be seen. (Patterns recorded with different sample detector distances.)

3.4 Membrane characterization by other methods

The H-GO and B-GO membranes prepared for this thesis were also analyzed using XPS (by other group members) which provided information about elemental composition, functionalization variety and impurities. The element compositions are mostly the same as for the pristine powder sample [12], but for B-GO membranes impurity of sodium was detected. This impurity comes from the NaOH solution used to dissolve the B-GO. Washing the B-GO membrane in a water-ethanol mixture results in decreasing amount of Na in the membranes below sensitivity of the method (<0.1%). It should be note that permeation tests performed for B-GO membranes were performed only for Na contaminated (not washed) as –prepared membranes.

Preliminary results, obtained using infrared spectroscopy, seem to confirm the trapping of water in the membrane structure and rather slow drying process.

3.5 Vapour permeation

One interesting feature of the GO membranes is their different permeability for different kinds of vapours. In this section the results of permeation experiments with water and ethanol vapour for pristine and heated membranes are presented. The permeation rate was measured using small liquid filled vial covered with membrane. The distance between liquid and membrane was about 1 cm so that the membrane is not in touch with liquid but exposed to vapour. Vapour absorbed by membrane on inner side of vial is evaporated after permeation on outer side of the membrane and the rate of evaporation is controlled by precise weight difference measurement from whole assemblage (details see section 2.3).

The H-GO membranes show similar behaviour similar to the one demonstrated by Nair et Al. [4]. **Fig. 42** shows raw data is plotted as weight difference vs. time for water, ethanol and reference experiments with open hole and hole sealed by aluminium foil using the same glue as used for membranes mounting. One can see that H_2O evaporation rate trough the membrane is close to that through an open hole and ethanol evaporation rates measured in two experiments are close to the one of the reference measurement with hole sealed by aluminium foil. It can also be observed that several experiments with ethanol show a strong deviation. For all the measurements silicone glue was used to attach membranes to vial cover and as it was discovered the glue did not allowed 100% sealing of the vial volume. However, experiments can approximately be corrected using reference experiment with aluminium foil used instead of GO membrane; the evaporation rate measured with this configuration can be used as (minimal) “zero point” background.

After heating the H-GO membrane at 145°C for one hour the evaporation rate of water dropped to the one of ethanol (see **Fig. 44**). The measurement was carried on for 16h and no change in the rate was measured.

For B-GO and water different behaviour was observed (**Fig. 43**). The water evaporation rate through the B-GO membrane is much smaller than the one through an open hole. For these measurements the membrane was glued with epoxy.

Summary of permeation rates observed for various membrane samples is given in **Fig. 45**. The data provided in this diagram are subjected to subtracting the (minimum) systematic error of due to leaking and normalization to the hole area.

The diagram shows that for H-GO the water vapour permeation rate is on the same level as trough the open hole, but B-GO membrane show an about 6 times slower water permeation rate. For ethanol vapour H-GO show permeation rates below the limits of measurement precision and B-GO membrane shows no significant permeation. Permeation completely stops even for slightly reduced membranes.

Some variation of the evaporation rates could possibly be connected to different leaking rates of assembled vial/membrane samples. Another important parameter is thickness of membranes which was poorly controlled in our experiments. Actual averaged thickness of produced membranes was estimated to be within 6-13 μm but exact correlation of permeation rates with thickness was not performed.

The lower evaporation rate of water through the B-GO membrane could be the result of more crystalline structure or the smaller interlayer d-spacing. The result of the XRD measurements show that for the heated membrane the interlayer-spacing is decreased which also results in absence of permeation.

The results of this sections show that for ethanol vapour the H-GO and B-GO membranes are not or very little permeable, but for water vapour they are permeable which is in agreement with the results of Nair et. Al. [4]. However the water vapour permeates much faster through the H-GO membrane then through the B-GO membrane. After heating for one hour the H-GO membrane is not permeable also for water vapour.

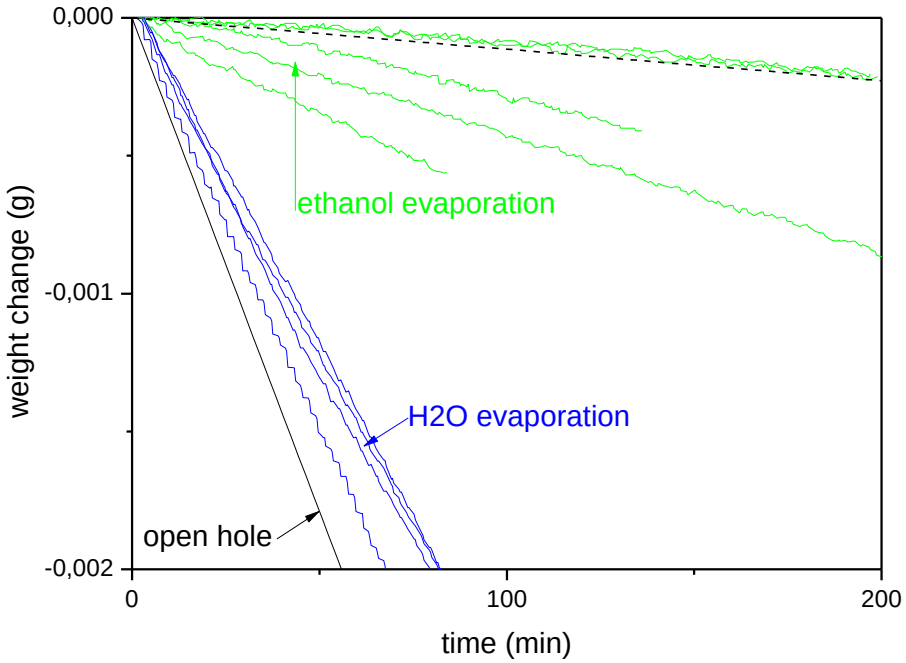


Fig. 42 Weight losses of evaporation-vials of over time. Evaporation-vials were filled with water (blue) and ethanol (green). The vials were closed with **H-GO membranes** by the use of **silicone glue**. The solid black line shows the weight loss of a vial with open hole filled by water. The black dashed line shows the average weight loss of a vial closed with an aluminum foil using silicone glue. Note: This are the untouched measurement results, the evaporation vials have different hole diameters and the error of silicon leaking is not subtracted.

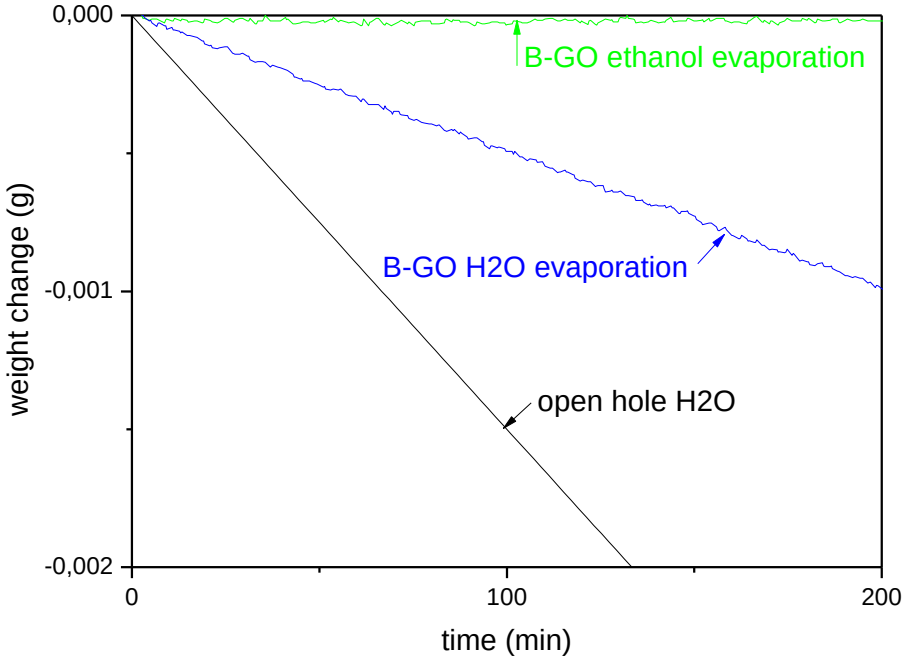


Fig. 43 Weight losses of evaporation-vials of over time. Evaporation-vials were filled with water (blue) and ethanol (green). The vial was closed with **B-GO membranes** by the use of **epoxy glue**. The solid black line shows the calculated weight loss of a vial with open hole with the same hole-area filled by water.

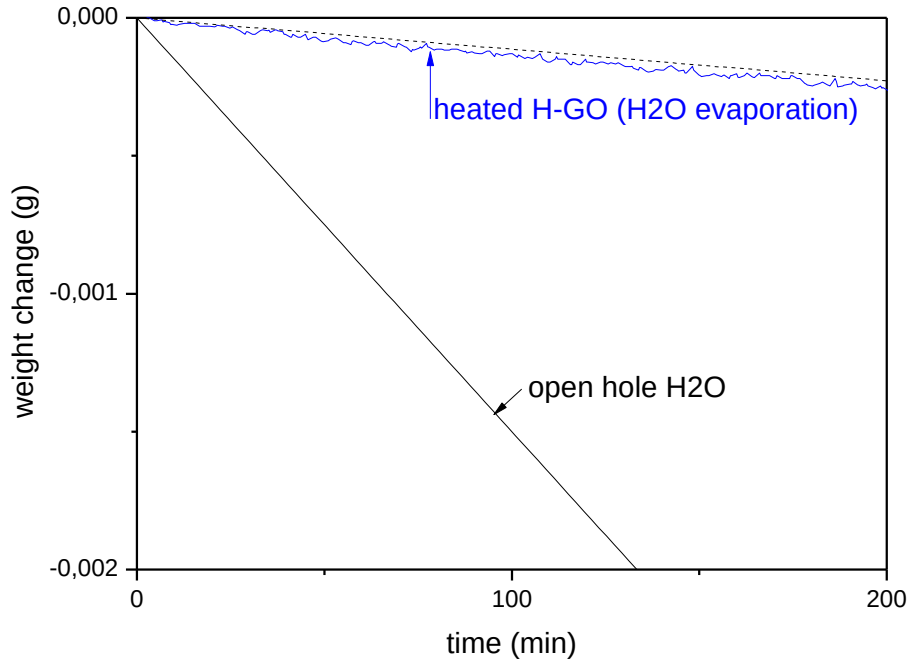


Fig. 44 Weight losses of evaporation-vials of over time. Evaporation-vials were filled with water (blue) closed with **B-GO membranes** by the use of **epoxy glue**. The solid black line shows the calculated weight loss of a vial with open hole with the same hole-area filled by water.

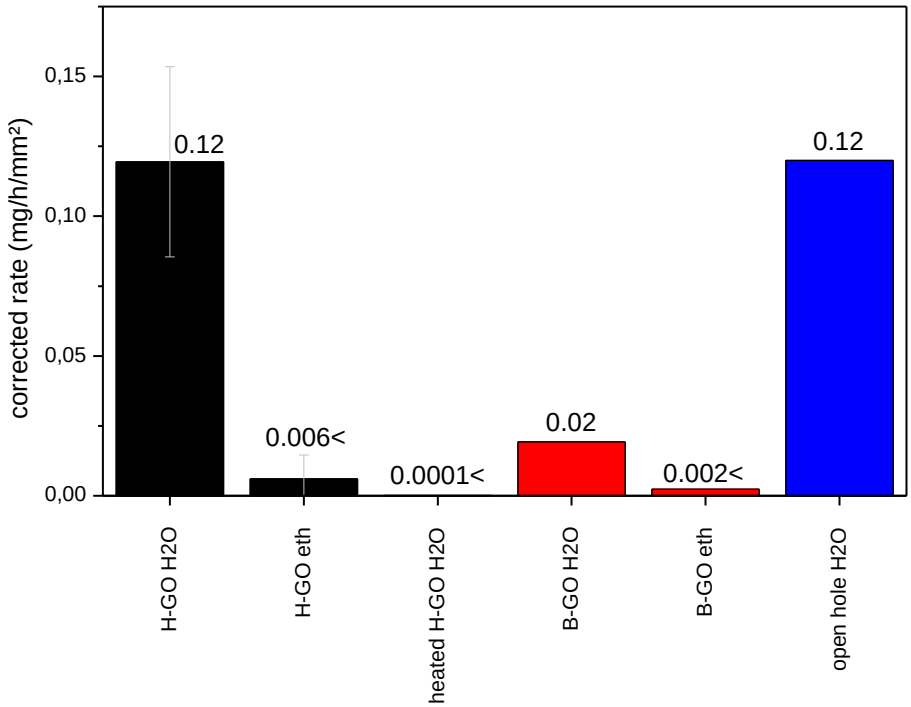


Fig. 45 Average of evaporation rates for water (H2O) and ethanol (eth) corrected by subtracting the leaking rate of the silicone (see section 2.3) and normalized to the area of the hole. The error bars show the standard deviation of the results if multiple measurements were available.

3.6 Permeation of liquid ethanol water mixture in filtering experiments

Since the permeability of membrane was found to be significantly different for water-vapour and ethanol-vapour, it is of interest to verify how a mixture of water and ethanol will permeate through the membrane. One of possible applications of membranes suggested in original study by Nair et al., [4] is separation of water from alcohols by passing through the membrane.

The ratio of a liquid water/ethanol-mixture is easier to control and to measure then a vapour mixture. Therefore, we were able to design simple liquid filtering experiment (see section 2.2) where the membrane is covered by liquid on the top and water evaporates form the bottom side of the membrane accelerated by vacuum. Two measurements were performed: one with H-GO and one with B-GO membrane. Concentration of ethanol was measured in the remaining liquid not yet passed through the membrane. The experiments were performed with ethanol- rich mixtures in order to verify if high purity ethanol can be obtained using the filtering.

The concentration measurements of the remaining mixture show that the ethanol concentration was increasing for both membranes (see **Fig. 46**). Some small loss of solvent in process of concentration measurements was unavoidable since about 2 ml of solution had to be withdrawn from the vial and it is not 100% of this amount which is returned back from the densitometer. The volume change in process of filtering measurements corrected to this error is shown in **Fig. 47.**

The filtering rate (volume per time) is clearly decreasing with higher concentrations of ethanol in the filtered mixture for B-GO membrane (see **Fig. 48**). For H-GO membrane the permeation rate also decreased, but was at a relatively high level also above 95% ethanol (see **Fig. 48**). It has to be considered that the membrane changed during the filtration process, which might result in variation of the permeation rate.

The change in a composition of remaining liquid mixture proves that water and ethanol permeate trough the membrane in different rates and the liquid which evaporates from the bottom side of the membrane (after passing trough) has different concentration of ethanol.

The average concentration of ethanol in the filtered mixture (C_F) can be calculated out of the concentration change of the remaining liquid (see section 2.2). If the concentration of the remaining (C_R) liquid does not change the concentration then both concentrations have to be the same of course ($C_R = C_F$). **Fig. 49** shows that for the H-GO membrane the concentrations of ethanol in the binary mixture before and after passing the membrane become more similar to each other in process of experiment when for ethanol concentration of the remaining mixture become higher. In other words, separation effect becomes smaller with time since the permeation rates of water and ethanol become more and more similar for highly purified ethanol with little remaining fraction of water. For B-GO the relative error of the volume measurement compared to the total volume was too big to see a clear trend.

It can be concluded that a mixture of water and ethanol is permeating through the membrane. However the ethanol concentration of the permeating liquid is lower than the concentration of the mixture on the membrane.

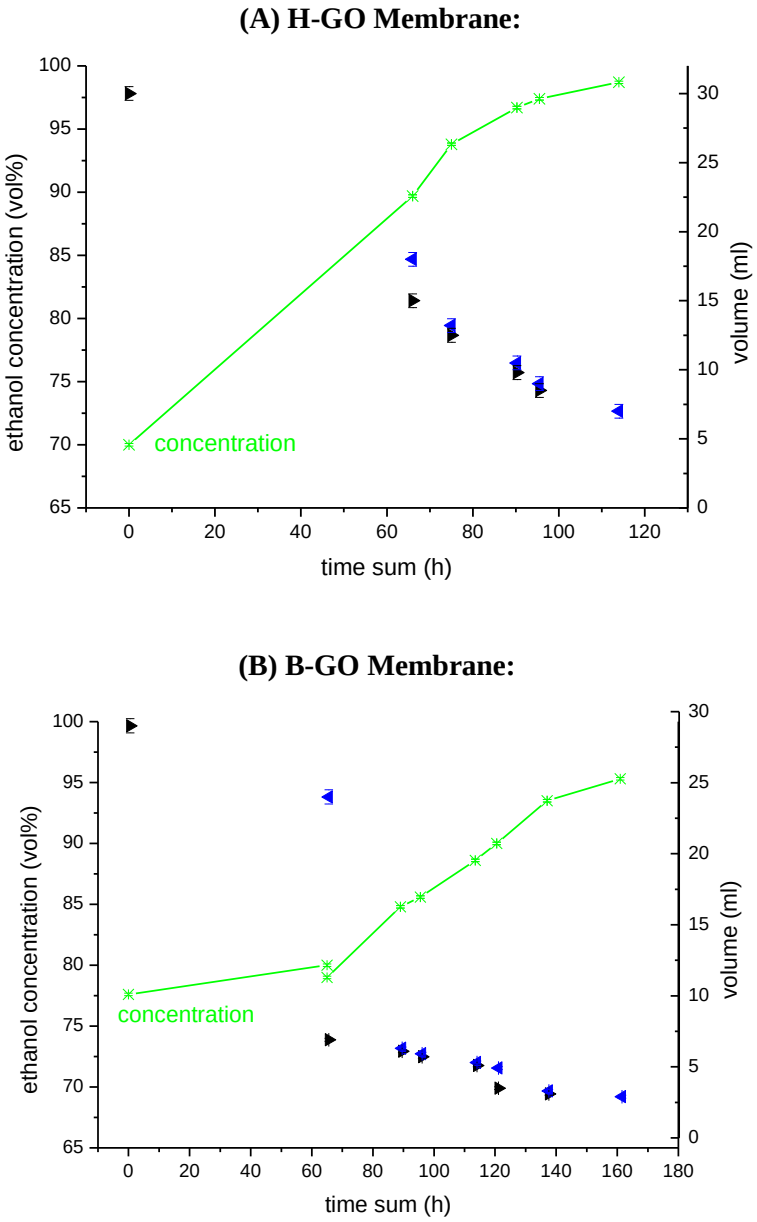
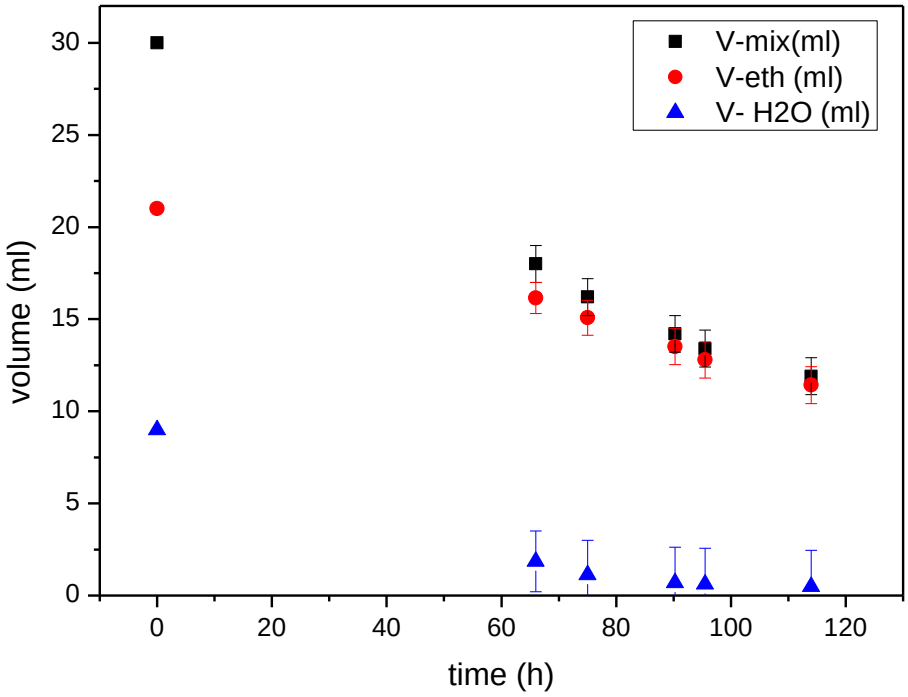


Fig. 46 Ethanol concentration (X–X) and remaining volume in syringe in process of filtering over time for H-GO membrane (A) and B-GO membrane (B). The Volume changes after concentration measurement: V_2 (◂) is before and V_1 (▸) after the concentration measurement at one point of time. Green lines are guidelines for the eye.

(A) H-GO Membrane:



(B) B-GO Membrane:

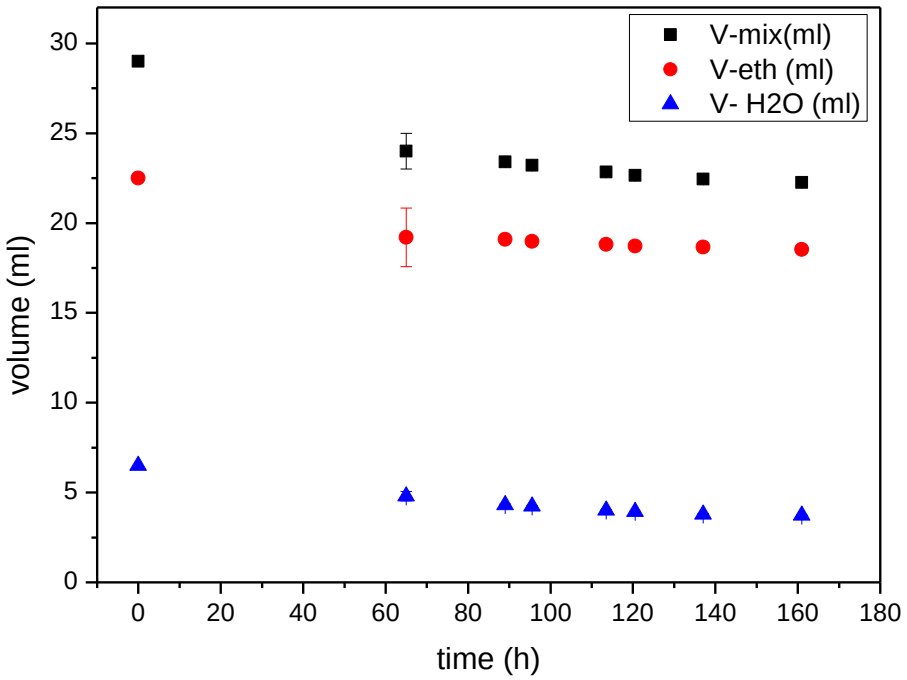


Fig. 47 Estimated volume change due to permeation trough the membrane (corrected values with subtracted losses due to concentration measurements). Total volume of remaining liquid (■), estimated volumetric fractions of ethanol (●) and water (▲). The error bars represent the maximum error due to inaccuracy of volume and concentration measurement.

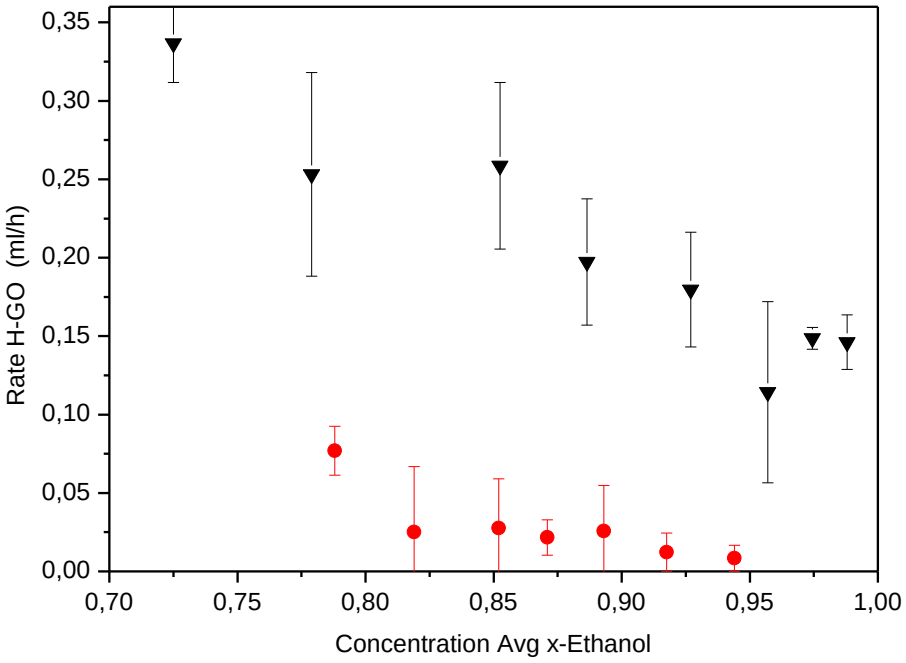


Fig. 48 Filtering rate of the total mixture for H-GO (▲) and B-GO (●) membranes.

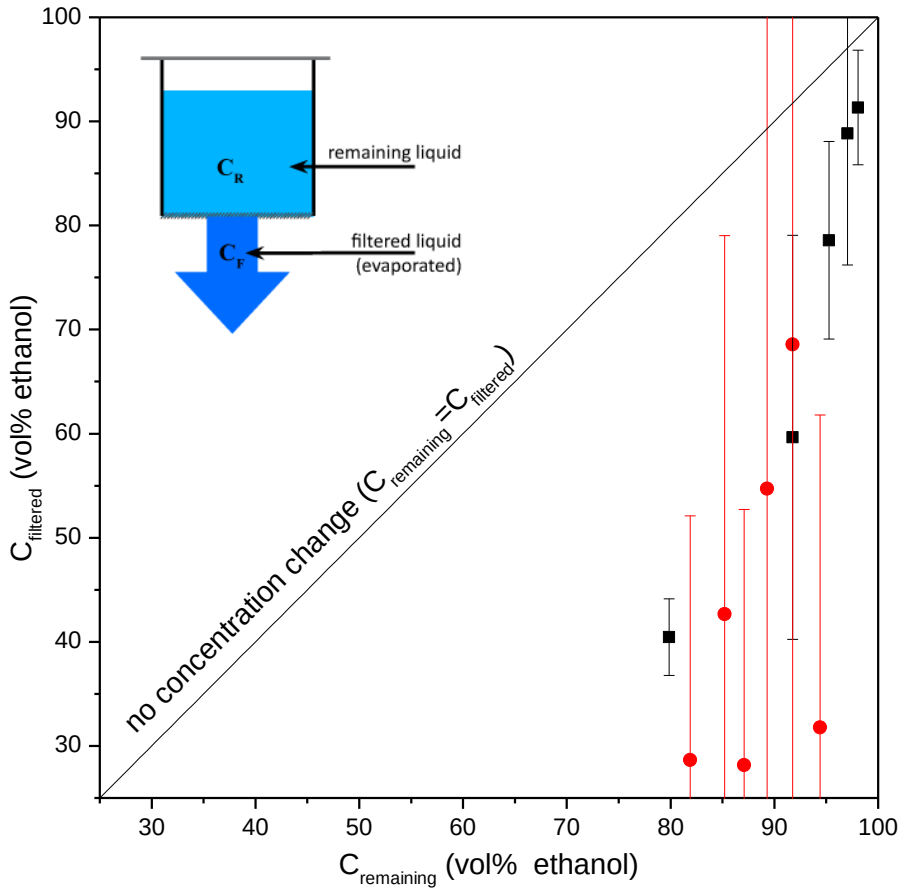


Fig. 49 Concentration of filtered mixture (C_F) over concentration of remaining mixture (C_R) for H-GO (■) and B-GO (●) membrane.

4 Summary and conclusion

Graphene oxide membrane synthesis, structural characterization and permeation properties were performed in this thesis. Three types of precursor graphite oxide were tested for membrane preparation: Membranes out of "Single Layer Hummers Graphite Oxide" (SL-H-GO), Hummers Graphite Oxide (H-GO) and Brodies Graphite oxide (B-GO) were synthesized and analyzed.

Main results of our studies can be summarized as following:

The membranes were grown using solutions of these pristine materials by controlled filtering according to procedures described in ref. [27],[4]. Similar to these earlier studies, membranes were prepared using Hummers graphite oxide. A new type of membrane was successfully prepared using Brodie graphite oxide dispersed in solution in slightly alkaline solution. SL-H-GO solution was found to be not suitable for preparation of homogenous membranes. The H-GO membranes are less transparent then the B-GO membranes. Growth time is shorter for H-GO then for B-GO membranes under same conditions of deposition.

XRD characterization shows that GO membranes consist of planar sheets stacked in approximately parallel orientation over the hole membrane. The microscopic ordering of these sheets is qualitatively similar to the one in pristine graphite oxide powders. However the (001)-d-spacing of freshly prepared membranes is slightly higher and decreases slowly under ambient conditions. After prolonged storing of the membranes for several weeks the interlayer spacing decreases to the value of pristine powder. For water immersed H-GO membranes the interlayer spacing increases similar to the spacing of pristine powder. While the H-GO membrane dries up, the interlayer spacing decreases to the value of freshly grown membranes within several hours. During the process of heating membranes the interlayer-distance decreases within the first hour stronger than in the hours afterwards.

For ethanol vapour the H-GO and B-GO membranes are not or very little permeable, but they are permeable for water vapour. Water vapour permeates much faster through the H-GO membrane (like through an open hole) and about 6 times slower through the B-GO membrane. After heating for one hour at 145°C the H-GO membrane is also not permeable also for water vapour.

Tests with ethanol-water mixtures with over $75\%_{vol}$ ethanol show that liquid ethanol water mixtures can permeate through the membrane. Both water and ethanol are able to permeate trough the membrane, but permeation rate of water is faster. The difference between permeation rates of water and ethanol exposed to binary liquid mixture decreases for compositions with higher fraction of ethanol. Therefore, efficiency of ethanol purification by passing through the membrane decreases as the concentration of ethanol goes over ~90-95%. Possible application of H-GO membrane for ethanol purification was successfully demonstrated by achieving 99% purity. However, the process of separation is rather slow and significant loss of ethanol on the later stages of purification were observed.

Based on these results the following conclusions can be drawn: From the XRD results can be concluded that the graphene flakes have a macroscopic parallel orientation. Furthermore the results show that water is more strongly trapped in the membrane structure then in the structure of pristine graphite oxide. The permeation tests show that GO-membrane properties can be influenced by choice of the precursor graphite oxide material. Finally it can be concluded that graphene oxide membranes are, in principle, suitable for purification of ethanol from ethanol/water mixtures. However, a set of problems needs to be addressed for practical applications. The main problems are that permeation rates of liquid ethanol and water for water/methanol mixtures are not sufficiently different and membranes are not sufficiently stable when in contact with liquid water/ethanol mixture.

5 Appendix

5.1 Data of GO solutions

Solution ID (=Sample)	GO Material	GO (mg)	H2O (ml)	Sonication time (h)	Centrifugate	Concentration (mg/ml)
Solution001	SL-H-GO	42	30	26	60min 8000RPM	
Solution002	SL-H-GO	31.4	30	22	60min 8000RPM	
Solution003	SL-H-GO	26.5	31	24	60min 8000RPM	0.7±0.07
Solution004	H-GO	34	41	27	60min 8000RPM	0.6±0.10
Solution005	H-GO	31	31	23	60min 8000RPM	0.6±0.14
Solution009	H-GO	12.5	22	24	110min 8000RPM	0.5±0.20
Solution007	B-GO	7.2	12.6		60min 4400RPM	
Solution012	B-GO	7.6	13.2	16	30min 4400RPM	1.3±0.18

Tab. 1 Solutions of Graphite Oxide materials. The Solution ID is used for references only.

5.2 Data of Membranes

Membrane ID	Solution ID	Solution (ml)	H2O Dilution (ml)	Approx. Filtering time (h)	Comment
1	2	10	0		Solution bypassed filter
2	2	16	0	1	
3	1	11	0	?	Solution Resonicated >38°C for 1 hour!
4	2	4.5	0	6.5	
5	2	3.3	2.7	5.5	
6	2	1.6	1.4	15	Pump on for 10 minutes only in the beginning
7	3	2	2	3	Delution test (see notes for details)
8	3	2.5	12.5	<16	Delution test (see notes for details)
9	3	2	20	20	Delution test (see notes for details)
10	3	2	10		Growing test (see notes)
11	3	2	10	8	added 2ml H2O to silange before filterholder was empty
13	4	4	0	2	
14	4	5	0	3.5	used Filter. 2ml H2O added when syringe was empty
15	4	6	0	28	pump on for short time. top grid of filter used. structure of top-grid visible on membrane
16	4	4.5	4.5	4.5	
17	4	6	6	22	
18	5	5	5	21	
19	5	4.5	4.5	24	added 2ml H2O in the end
20	5	3	3	<20	

Membrane ID	Solution ID	Solution (ml)	H2O Dilution (ml)	Approx. Filtering time (h)	Comment
21	5	2	2	6	
22	5	2	3+8ml later		ETHANOL+H2O permeation test 1
23	5	2	2	6	
24	5	2	2	6	
25	7	3		2.5	
26	7	4		5.5	
27	6	?(6)			liquid bypassed filter
28	8	?(3.5)			liquid bypassed filter
29	7	2.4			eth/water mix test
30	11	4			eth/water mix test
32	11	4		3	liquid bypassed filter
33	11	4			liquid bypassed filter/filter broken
34	11	3		4	incl top grid
35	11	4		7	
36	12	4		4	
37	12	?(3)			liquid bypassed filter
38	9	4		1	
39	9	4		1.5	

Tab. 2 Details of Membrane synthesis. H2O Delution gives the added volume of H2O for diluting.

6 References

[1] A. K. Geim and K. S. Novoselov, "The rise of graphene," *Nat. Mater.*, no. 6, p. 183, 2007.

[2] D. R. Dreyer, S. Park, C. W. Bielawski and R. S. Ruoff, "The chemistry of graphene oxide," *Chem. Soc. Rev.*, no. 39, p. 228, 2010.

[3] H. Boehm, A. Clauss and U. Hofmann, "Graphite oxide and its membrane properties," *J. Chim. Phys. Rev. Gen.*, no. 58, p. 141, 1961.

[4] R. R. Nair, H. A. Wu, P. N. Jayaram, I. V. Grigorieva and A. K. Geim, "Unimpeded Permeation of Water Through Helium-Leak-Tight Graphene-Based Membranes," *Science*, no. 335, p. 442, 2012.

[5] B. C. Brodie, "On the Atomic Weight of Graphite," *Pil. Trans.*, no. 149, p. 249, 1859.

[6] W. S. Hummers and R. E. Offeman, "Preparation of Graphitic Oxide," *J. Am. Chem Soc.*, no. 80, p. 1339, 1958.

[7] T. Szabo, V. Hornok, R. A. Schoonheydt and I. Dekany, "Hybrid Langmuir-Blodgett monolayers of graphite oxide nanosheets," *Carbon*, no. 48, p. 1676, 2010.

[8] Y. W. Zhu, W. W. Cai, R. D. Piner, A. Velamakanni and R. S. Ruoff, "Transparent self-assembled films of reduced graphene oxide platelets," *Appl. Phys. Lett.*, no. 95, 2009.

[9] L. Staudenmaier, "Verfahren zur Darstellung der Graphitsäure," *Ber. Dtsch. Chem. Ges.*, no. 31, p. 1481, 1898.

[10] T. Szabó, O. Berkesi, P. Forgó, K. Josepovits, Y. Sanakis, D. Petridis and I. Dékány, "Evolution of Surface Functional Groups in a Series of Progressively Oxidized Graphite Oxides," *Chem. Mater.*, no. 18, p. 2740, 2006.

[11] H. Te, T. Riedl, A. Lerf and J. Klinowski, "Solid-State NMR Studies of the Structure of Graphite Oxide," *J. Phys. Chem*, no. 100, p. 19954, 1996.

[12] S. You, S. M. Luzan, T. Szabó and A. V. Talyzin, "Effect of synthesis method on solvation and exfoliation of graphite oxide," *Carbon*, no. 52, p. 171, 2013.

[13] D. Paciléa, J. Meyerb, A. F. Rodríguezc, M. Papagnod, C. Gómez-Navarroe, R. Sundarame, M. Burgharde, K. Kerne, C. Carboned and U. Kaiserb, "Electronic properties and atomic structure of graphene oxide membranes," *Carbon*, no. 49, p. 966,

2011.

[14] A. Buchsteiner, A. Lerf and J. Pieper, “Water Dynamics in Graphite Oxide Investigated with Neutron Scattering,” *J. Phys Chem. B,* no. 110, p. 22328, 2006.

[15] A. Lerf, A. Buchsteiner, J. Pieper, S. Schottl, I. Dekany, T. Szabo and H. P. Boehm, “Hydration Behavior and Dynamics of Water Molecules in Graphite Oxide,” *J. Phys. Chem. Solids,* no. 67, p. 1106, 2006.

[16] R. Bergman and J. Swenson, “Dynamics of supercooled water in confined geometry,” *Nature,* no. 403, pp. 283-286, 2000.

[17] S. Cerveny, F. Barroso-Bujans, Á. Alegría and J. Colmenero, “Dynamics of Water Intercalated in Graphite Oxide,” *J. Phys. Chem. C,* no. 114, p. 2604, 2010.

[18] A. Lerf, H. He, M. Forster and J. Klinowski, “Structure of Graphite Oxide Revisited,” *J. Phys. Chem. B,* no. 102, p. 4477, 1998.

[19] A. V. Talyzin, B. Sundqvist, T. Szabo, I. Dekany and V. Dmitriev, “Pressure-induced insertion of liquid alcohols into graphite oxide structure.,” *J Am Chem Soc,* no. 131(51), p. 18445, 2009.

[20] S. You, S. Luzan, J. Yu, B. Sundqvist and A. V. Talyzin, “Phase transitions in graphite oxide solvates at temperatures near ambient,” *J Phys Chem Lett,* no. 3, p. 812, 2012.

[21] S. You, J. Yu, B. Sundqvist and A. V. Talyzin, “Solvation of graphite oxide in water–methanol binary polar solvents,” *Phys. Status Solidi B,* no. 249, 2012.

[22] Y. Si and E. T. Samulski, “Synthesis of Water Soluble Graphene,” *Nano Lett.,* no. 8, p. 1679, 2008.

[23] H. A. Becerril, J. Mao, Z. Liu, R. M. Stoltenberg, Z. Bao and Y. Chen, “Evaluation of solution-processed reduced graphene oxide films as transparent conductors,” *ACS nano,* no. 2, p. 463, 2008.

[24] N. I. Kovtyukhova, P. J. Ollivier, B. R. Martin, T. E. Mallouk, S. A. Chizhik, E. V. Buzaneva and A. D. Gorchinskiy, “Layer-by-layer assembly of ultrathin composite films from micron-sized graphite oxide sheets and polycations,” *Chem. Mater.,* no. 11, p. 771, 1999.

[25] C. Gómez-navarro, R. T. Weitz, A. M. Bittner, M. Scolari, A. Mews, M. Burghard and K. Kern, “Electronic transport properties of individual chemically reduced graphene oxide sheets,” *Nano Lett.,* no. 9, p. 2206, 2007.

[26] X. Wen, C. W. Garland, T. Hwa, M. Kardar, E. Kokufuta, Y. Li, M. Orkisz and T. Tanaka, “Crumpled and collapsed conformation in graphite oxide membranes,” *Nature,*

no. 355, p. 426, 1992.

[27] D. A. Dikin, S. Stankovich, E. J. Zimney, R. D. Piner, G. H. B. Dommett, G. Evmenenko, S. T. Nguyen and R. S. Ruoff, “Preparation and characterization of graphene oxide paper,” *Nature,* no. 448, p. 457, 2007.

[28] I. Jung, M. Vaupel, M. Pelton, R. Piner, D. A. Dikin, S. Stankovich, J. An and R. S. Ruoff, “Characterization of Thermally Reduced Graphene Oxide by Imaging Ellipsometry,” *J. Phys. Chem. C,* no. 112, p. 8499, 2008.

[29] C. Chengmeng, Y. Quan-Hong, Y. Yonggang, L. Wei, W. Yuefang, H. Peng-Xiang, W. Maozhang and C. Hui-Ming, “Self-Assembled Free-Standing Graphite Oxide Membrane,” *Adv. Mater.,* no. 21, p. 3007–3011, 2009.

[30] M. Krueger, S. Berg, D. Stone, E. Strelcov, D. A. Dikin, J. Kim, L. J. Cote, J. Huang and A. Kolmakov, “Drop-Casted Self-Assembling Graphene Oxide Membranes for Scanning Electron Microscopy on Wet and Dense Gaseous Samples,” *acs nano,* no. 12, p. 10047, 2011.

[31] S. Gilje, S. Han, M. Wang, K. L. Wang and R. B. Kaner, “A chemical route to graphene for device applications,” *Nano lett.,* no. 7, p. 3394, 2007.

[32] S. Pang, H. N. Tsao, X. Feng and K. Müllen, “Patterned Graphene Electrodes from Solution-Processed Graphite Oxide Films for Organic Field-Effect Transistors,” *Adv. mat.,* no. 21 , p. 3488, 2009.

[33] J. T. Robinson, M. Zalalutdinov, J. W. Baldwin, E. S. Snow, Z. Wei, P. Sheehan and B. H. Houston, “Wafer-scale reduced graphene oxide films for nanomechanical devices,” *Nano lett.,* no. 8, p. 3441, 2008.

[34] V. Lee, L. Whittaker, C. Jaye, K. Baroudi, D. Fischer and S. Banerjee, “Large-Area Chemically Modified Graphene Films: Electrophoretic Deposition and Characterization by Soft X-ray Absorption Spectroscopy,” *Chem. Mater.,* no. 21, p. 3905, 2009.

[35] G. Eda and M. Chhowalla, “Chemically Derived Graphene Oxide: Towards Large-Area Thin-Film Electronics and Optoelectronics,” *Adv. Mater.,* no. 22, p. 2392, 2010.

[36] P. Z. Sun, M. Zhu, K. L. Wang, M. L. Zhong, J. Q. Wei, D. H. Wu, Z. P. Xu and H. W. Zhu, “Selective Ion Penetration of Graphene Oxide Membranes,” *Acs Nano,* no. 7, p. 428, 2013.

[37] K. Feng, B. B. Tang and P. Y. Wu, “"Evaporating" Graphene Oxide Sheets (GOSs) for Rolled up GOSs and Its Applications in Proton Exchange Membrane Fuel Cell.,” *Acs Appl. Mater. Inter.,* no. 5, p. 1481, 2013.

[38] J. M. Zhu, L. W. Zhu, Z. F. Lu, L. Gu, S. L. Cao and X. B. Cao, "Selectively Expanding Graphene Oxide Paper for Creating Multifunctional Carbon Materials," *J Phys. Chem. C,* no. 116, p. 23075, 2012.

[39] N. M. Martin, Synthesis of carbon nanomaterials using fullerenes as a precursor, Umeå University, Sweden: Master Thesis from Department of Physics (supervisor- A.Talyzin), 2009.

[40] J. D. Patterson and B. C. Bailey, Solid-state physics : introduction to the theory, Berlin : Springer , 2007.

[41] C. Kittel, Introduction to solid state physics, New York: Wiley , 2005 .

[42] N. W. Ashcroft and N. D. Mermin, Festkörperphysik, 4 ed., München: Oldenbourg Verlag, 2013.

[43] M. S. Rogalski and S. B. Palmer, Solid state physics, Amsterdam: OPA, Gordon & Breach, 2000.

[44] W. H. Bragg and W. L. Bragg, "The Reflection of X-rays by Crystals," *Proc. R. Soc. Lond.,* no. 88, p. 428, 1913.

[45] P. A. Schroeder, "Lecture notes for Clay Mineralogy," [Online]. Available: http://www.gly.uga.edu/Schroeder/geol6550/CM13.html. [Accessed 25 February 2013].

[46] V. A. Drits and D. K. McCarty, "The nature of diffraction effects from illite and illite-smectite consisting of interstratified trans-vacant and cis-vacant 2:1 layers: A semiquantitative technique for determination of layer-type content," *American Mineralogist,* no. 81, p. 852, 1996.

[47] M. Garcia-Gutierrez and D. Rueda, "Bases of Synchrotron Radiation, Light Sources, and Features of X-Ray Scattering Beamlines," in *Applications of Synchrotron Light to Scattering and Diffraction in Materials and Life Science,* vol. 776, SPRINGER-VERLAG BERLIN, 2009, pp. 1-22.

[48] E. Koch, "Trigonal and hexagonal crystal system," in *International Tables for Crystallography,* vol. C, 2006, p. 6.

[49] D. Chung, "Review Graphite," *J. Mater. Sci,* no. 8, p. 1475, 2002.

[50] E. Ryschkewitsch, Graphit, Leipzig: Hirzel, 1926.

[51] Z. Li, C. Lu, Z. Xia, Y. Zhou and Z. Luo, "X-ray diffraction patterns of graphite and turbostratic carbon," *Carbon,* no. 45, p. 1686, 2007.

[52] J. R. Helliwell, “Single-crystal X-ray techniques,” in *International Tables for Crystallography*, C ed., 2006, pp. 26-41.

[53] Y. Cerenius, K. Stahl, L. A. Svensson, a. T. Ursby, A. Oskarsson, J. Albertssond and A. Liljasa, “The crystallography beamline I711 at MAX II,” *J. Synchrotron Rad.*, no. 7, p. 203, 2000.